



Crustal growth at active continental margins: Numerical modeling

Katharina Vogt^{a,*}, Taras V. Gerya^{a,b}, Antonio Castro^c

^a Geophysical Fluid Dynamics Group, Institute of Geophysics, Department of Earth Sciences, Swiss Federal Institute of Technology (ETH-Zurich), Sonneggstrasse, 5, 8092 Zurich, Switzerland

^b Adjunct Professor of Geology Department, Moscow State University, 119899 Moscow, Russia

^c Department of Geology, University of Huelva, Spain

ARTICLE INFO

Article history:

Received 3 July 2011

Received in revised form 15 December 2011

Accepted 23 December 2011

Available online 5 January 2012

Keywords:

Crustal growth

Magmatic addition

Active continental margins

Numerical modeling

ABSTRACT

The dynamics and melt sources for crustal growth at active continental margins are analyzed by using a 2D coupled petrological–thermomechanical numerical model of an oceanic–continental subduction zone. This model includes spontaneous slab retreat and bending, dehydration of subducted crust, aqueous fluid transport, partial melting, melt extraction and melt emplacement in form of extrusive volcanics and intrusive plutons. We could identify the following three geodynamic regimes of crustal growth: (i) stable arcs, (ii) compressional arcs with plume development, and (iii) extensional arcs. Crustal growth in a stable subduction setting results in the emplacement of flattened intrusions in the lower crust. At first dacitic melts, extracted from partially molten rocks located atop the slab (gabbros and basalts), intrude into the lower crust followed by mantle-derived (wet peridotite) basaltic melts from the mantle wedge. Thus extending plutons form in the lower crust, characterized by a successively increasing mantle component and low magmatic addition rates (10 km³/km/Myrs). Compressional arcs are accomplished by the formation and emplacement of hybrid plumes. In the course of subduction localization and partial melting of basalts and sediments along the slab induces Rayleigh Taylor instabilities. Hence, buoyant plumes are formed, composed of partially molten sediments and basalts of the oceanic crust. Subsequently, these plumes ascend, crosscutting the lithosphere before they finally crystallize within the upper crust in form of silicic intrusions. Additionally, intrusions are formed in the lower crust derived by partial melting of rocks located atop the slab (basalts, gabbros, wet peridotite) and inside the plume (basalts, sediments). Magmatic addition rates are somewhat higher compared to stable arcs (40–70 km³/km/Myrs). Subduction in an extensional arc setting results in decompression melting of dry peridotite. The backward motion of the subduction zone relative to the motion of the plate leads to thinning of the overriding plate. Thus, hot and dry asthenosphere rises into the neck as the slab retreats, triggering decompression melting of dry peridotite. Consequently large volumes of mafic (oceanic) crust are formed in the backarc region with total magmatic addition rates being as high as 90–170 km³/km/Myrs.

© 2012 Elsevier B.V. All rights reserved.

1. Introduction

The vast variety of igneous rocks of the continental crust implies that magmatism and crustal growth are closely linked to different geodynamic settings. Present day crustal growth is ascribed to two distinct plate tectonic settings: intraplate and convergent margins (Rudnick, 1995). Here we focus on crustal growth at continental margins, where oceanic crust is subducted beneath the continental lithosphere. The bulk composition of the continental crust is andesitic and cannot be derived directly by partial melting of the mantle (Rudnick, 1995; Hawkesworth and Kemp, 2006). Different mechanisms of crust formation have been proposed by scientists facing this problem (e.g., Taylor, 1966; Taylor and McLennan, 1985; Green,

1980; Ringwood, 1989; Kay and Kay, 1991; Rudnick, 1995; Tatsumi, 2005). Understanding the dynamics of crustal growth requires identification of melt sources and estimates on the proportions of magmas derived from different sites of production, which add to the growth of the continental crust. Three potential sources of melt production can be identified: the mantle, subducted oceanic crust and continental crust, which experience melting under different physical conditions (Wyllie, 1984). It is widely accepted that water released from the subducting plate lowers the melting temperature of the overlying mantle allowing for “flux melting” of the hydrated mantle (e.g., Stolper and Newman, 1994; Tatsumi and Eggs, 1995; Schmidt and Poli, 1998; Iwamori, 1998). The role of slab derived melts is strongly debated in the literature, because subducted oceanic crust of most modern subduction zones is believed to be too cold to permit slab melting (Schmidt and Poli, 1998; Peacock et al., 1994). Nevertheless it has been argued, that the formation of slab

* Corresponding author.

E-mail address: katharina.vogt@erdw.ethz.ch (K. Vogt).

derived melts is possible for young subduction zones (Kay, 1978; Drummond and Defant, 1990; Defant and Drummond, 1990; Sajona et al., 1993). A general problem of crustal production processes within subduction zones is the relation of geodynamics to the composition of newly formed crust. The transition between different geodynamic regimes is closely linked to weakening effects imposed by fluids and melts (Gerya and Meilick, 2011) and has a major influence on arc growth. However, previous crustal growth models (e.g., Nikolaeva et al., 2008; Gerya and Meilick, 2011) neglected possible geodynamic effects of the overriding plate motion (e.g., van Hunen et al., 2000, 2002; Heuret et al., 2007; Sobolev and Babeyko, 2005; Schellart, 2008) and/or intrusion emplacement, which leaves a significant gap in our understanding of crustal growth processes within subduction zones.

In order to fill in these gaps and investigate sites of melt production and crustal growth in relation to different geodynamic scenarios we performed a series of 2D numerical experiments by using a coupled petrological–thermomechanical numerical model of an oceanic–continental subduction zone. The model includes overriding plate motion, spontaneous slab bending, dehydration of subducted crust, aqueous fluid transport, partial melting, melt extraction and melt emplacement in form of extrusive volcanics and intrusive plutons.

2. Numerical model description

2.1. Model setup

The 2D coupled petrological–thermomechanical model simulates forced subduction of an active continental margin. A lithospheric to upper mantle cross-section of a subduction zone is modeled by an area of 4000 km by 200 km within a 50 Myrs time span (Fig. 1). At an imposed convergence rate of 5 cm/year or 3 cm/year, for varying upper plate velocities the oceanic plate (2500 km)

is pushed toward an either fixed or moving continental plate (1500 km) reproducing a collision zone.

The rectangular grid with 2041 * 201 nodes is non-uniform, resulting in a high resolution (1 km * 1 km) area in the center of the model covering 1500 km horizontally, while the rest of the model remains at a lower resolution (5 * 1 km). The oceanic crust consists of 2 km of hydrated basalts and 5 km of gabbros. The continental crust is felsic and has a total thickness of 30 km. Both the asthenosphere and the upper mantle are composed of anhydrous peridotite and are defined by the temperature profile. For detailed material properties see Table 1. Water release and consumption as a function of pressure and temperature are computed from thermodynamic data by Gibbs free energy minimization (Connolly, 2005; Gerya and Meilick, 2011). Initialization of subduction is prescribed by a rheologically weak shear zone (wet olivine) with low plastic strength ($\sin(\varphi) = 0.1$, where φ is the effective internal friction angle) at the bottom of the continental crust. Atop the border of the two plates accretionary sediments are settled. Oceanic plate advance is enabled by an internally prescribed velocity field within the convergence condition region. Bending of the subducting slab is spontaneous (Gorczyk et al., 2007).

All mechanical boundary conditions are free slip only the lower boundary being permeable (Gorczyk et al., 2007). The top surface of the lithosphere is treated as an internal free surface by using a top layer (of 8–12.5 km thickness) with low viscosity (10^{18} Pas) and low density (1 kg/m^3 for air, 1000 kg/m^3 for sea water). The large viscosity contrast across this boundary minimizes shear stresses ($<10^5 \text{ Pa}$) at the top of the lithosphere making it an efficient free surface (Schmeling et al., 2008). The topography of the boundary changes due to erosion and sedimentation according to the following Eulerian transport equation (Gorczyk et al., 2007):

$$\partial y_{es} / \partial t = v_y - v_x \partial y_{es} / \partial x - v_s + v_e,$$

where y_{es} is the vertical position of the surface as a function of the horizontal distance x ; v_y and v_x are the vertical and horizontal

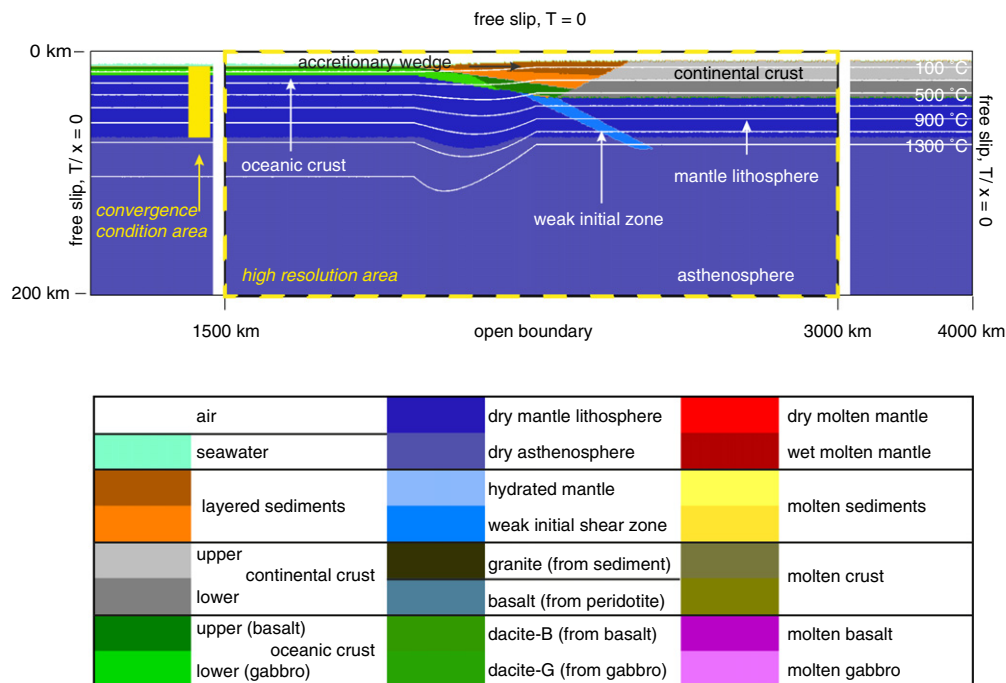


Fig. 1. Initial Setup of the numerical model (see text (Section 2.1) for details). Staggered grid resolution is 2041 × 201 nodal points, with more than 10 million randomly distributed markers. Grid step is 1 × 1 km in the subduction zone area (1500–3000 km) and 5 × 1 km outside of this area. Isotherms are displayed in white for increments of 200 °C, starting from 100 °C. Colors indicate materials (i.e. rock type or melt), which appear in subsequent figures. To illustrate deformation, two layers with the same physical properties are distinguished using different colors for sediments, crust (upper and lower crust) and mantle (asthenosphere and lithosphere).

Table 1
Physical properties of rocks^a used in numerical experiments.

Material	ρ_0 , kg/m ³	k , W/(m K) (at T_K , P_{MPa})	T_{solidus} , K (at P_{MPa})	T_{liquidus} , K (at P_{MPa})	Latent heat, kJ/kg	H_r , $\mu\text{W}/\text{m}^3$	Flow law
Sediments, volcanics from sediments	2600 (solid)2400 (molten)	$[0.64 + 807/(T + 77)] \times \exp(0.00004 \cdot P_{\text{MPa}})$	$889 + 17900/(P + 54) + 20200/(P + 54)^2$ at $P < 1200$ MPa, $831 + 0.06P$ at $P > 1200$ MPa	$1262 + 0.09P$	300	2	Wet quartzite, $c = 10$ MPa, $\sin(\varphi_{\text{dry}}) = 0.15$
Upper continental crust	2700 (solid)2400 (molten)	$[0.64 + 807/(T + 77)] \times \exp(0.00004 \cdot P_{\text{MPa}})$	$889 + 17900/(P + 54) + 20200/(P + 54)^2$ at $P < 1200$ MPa, $831 + 0.06P$ at $P > 1200$ MPa	$1262 + 0.09P$	300	1	Wet quartzite, $c = 10$ MPa, $\sin(\varphi_{\text{dry}}) = 0.15$
Lower continental crust	2700 (solid)2400 (molten)	$[0.64 + 807/(T + 77)] \times \exp(0.00004 \cdot P_{\text{MPa}})$	$973 - 70400/(P + 354) + 77800000/(P + 354)^2$ at $P < 1600$ MPa, $935 + 0.0035P + 0.0000062P^2$ at $P > 1600$ MPa	$1423 + 0.105P$	380	1	Wet quartzite, $c = 10$ MPa, $\sin(\varphi_{\text{dry}}) = 0.15$
Upper oceanic crust (basalt)	3000 (solid)2900 (molten)	$[1.18 + 474/(T + 77)] \times \exp(0.00004 \cdot P_{\text{MPa}})$	$973 - 70400/(P + 354) + 77800000/(P + 354)^2$ at $P < 1600$ MPa, $935 + 0.0035P + 0.0000062P^2$ at $P > 1600$ MPa	$1423 + 0.105P$	380	0.25	Wet quartzite, $c = 10$ MPa, $\sin(\varphi_{\text{dry}}) = 0.1$
Lower oceanic crust (gabbro)	3000 (solid)2900 (molten)	$[1.18 + 474/(T + 77)] \times \exp(0.00004 \cdot P_{\text{MPa}})$	$973 - 70400/(P + 354) + 77800000/(P + 354)^2$ at $P < 1600$ MPa, $935 + 0.0035P + 0.0000062P^2$ at $P > 1600$ MPa	$1423 + 0.105P$	380	0.25	Plagioclase An ₇₅ , $c = 10$ MPa, $\sin(\varphi_{\text{dry}}) = 0.6$
Volcanics from wet molten mantle and subducted basalts and gabbro	3000 (solid)2900 (molten)	$[1.18 + 474/(T + 77)] \times \exp(0.00004 \cdot P_{\text{MPa}})$	$973 - 70400/(P + 354) + 77800000/(P + 354)^2$ at $P < 1600$ MPa, $935 + 0.0035P + 0.0000062P^2$ at $P > 1600$ MPa	$1423 + 0.105P$	380	0.25	Wet quartzite, $c = 10$ MPa, $\sin(\varphi_{\text{dry}}) = 0.15$
Lithosphere–asthenosphere dry mantle	3300 (solid)2900 (molten)	$[0.73 + 1293/(T + 77)] \times (1 + 0.00004P)$	$1394 + 0.132899P - 0.000005104P^2$ at $P < 10000$ MPa, $2212 + 0.030819(P - 10000)$ at $P > 10000$ MPa	$2073 + 0.114P$	400	0.022	Dry olivine, $c = 10$ MPa, $\sin(\varphi_{\text{dry}}) = 0.6$
Lithosphere–asthenosphere wet mantle	3000 (serpentinized)3200 (hydrated)2900 (molten)	$[0.73 + 1293/(T + 77)] \times (1 + 0.00004P)$	$1240 + 49800/(P + 323)$ at $P < 2400$ MPa, $1266 - 0.0118P + 0.0000035P^2$ at $P > 2400$ MPa	$2073 + 0.114P$	400	0.022	10^{18} [Pas] wet olivine, $c = 10$ MPa, $\sin(\varphi_{\text{dry}}) = 0.1$
References ^b	1, 2	3, 9	4, 5, 6, 7, 8	4	1, 2	1	10

^a Other properties (for all rock types): $C_p = 1000 \text{ J kg}^{-1} \text{ K}^{-1}$, $\alpha = 3 \times 10^{-5} \text{ K}^{-1}$, $\beta = 1 \times 10^{-5} \text{ MPa}^{-1}$.

^b 1, Turcotte and Schubert (2002); 2, Bittner and Schmelting (1995); 3, Clauser and Huenges (1995); 4, Schmidt and Poli (1998); 5, Hess (1989); 6, Hirschmann (2000); 7, Johannes (1985); 8, Poli and Schmidt (2002); 9, Hofmeister (1999); 10, Ranalli, 1995.

components of the material velocity vector at the surface (y is positive downward, $y = 0$ at the top of the box); v_s and v_e are the sedimentation and erosion rates, respectively, which are defined as follows (Gerya and Meilick, 2011):

$$v_s = 0 \text{ mm/a} \quad v_e = 0.3 \text{ mm/a} \quad \text{for } y < 9 \text{ km}$$

$$v_s = 0.03 \text{ mm/a} \quad v_e = 0 \text{ mm/a} \quad \text{for } y < 10 \text{ km}.$$

In regions with steep surfaces, for example in the trench region, an increased erosion/sedimentation rate (1 mm/a) is used to account for additional mass transport in regions with steep topography slopes.

2.2. Hydration process

Connate water carried into subduction zones is expelled due to compaction and dehydration reactions in the course of subduction. Free fluid present in sediments and basalts makes up to 2 wt.% at the surface and is believed to decrease with depth. To account for compaction it is supposed that this water is released, decreasing from 2 wt.% to 0 wt.% at 75 km depth:

$$X_{\text{H}_2\text{O}(\text{wt}\%)} = (1 - 0.013 \cdot \Delta y) \cdot X_{\text{H}_2\text{O}(p_0)},$$

where $X_{\text{H}_2\text{O}(p_0)} = 2 \text{ wt}\%$ is the connate water content at the surface, and Δy is depth below the surface in km (0–75 km). Dehydration reactions and therewith associated water release are computed based on the physicochemical conditions and the assumption of thermodynamic equilibrium (Gorczyk et al., 2007; Nikolaeva

et al., 2008; Sizova et al., 2010; Gerya and Meilick, 2011). Once free fluid is released it propagates upward into the mantle wedge. This process is modeled in form of markers. Expelled water is stored in a newly generated water marker and moves independently upward according to (Gorczyk et al., 2007):

$$v_{x(\text{water})} = v_x, \quad v_{y(\text{water})} = v_y - v_{y(\text{percolation})},$$

where v_x and v_y describe the local velocity of the mantle and $v_{y(\text{percolation})}$ indicates the relative velocity of the upward percolation of the fluid ($v_{y(\text{percolation})} = 10 \text{ cm/a}$). If a given water marker encounters a lithology capable of absorbing water by hydration or partial melting, moving water is consumed. As suggested by seismic data (Carlson and Miller, 2003), an incomplete hydration of the mantle wedge of 2 wt.% is assumed as a consequence of channelization of slab-derived fluids (Davis, 1999).

2.3. Partial melting and melt extraction

In the model the mantle solidus is intermediate between the wet and dry peridotite solidi due to incomplete hydration. In nature, variable hydration triggers melting over a range of temperatures. Therefore it is assumed, that the degree of both hydrous and dry melting is a linear function of pressure and temperature (e.g., Gerya and Yuen, 2003). For a given pressure and rock composition the volumetric degree of melting M_0 is:

$$M_0 = 0 \quad \text{when } T < T_{\text{solidus}},$$

$$M_0 = (T - T_{\text{solidus}})/(T_{\text{liquidus}} - T_{\text{solidus}}) \quad \text{when } T_{\text{solidus}} < T < T_{\text{liquidus}},$$

$$M_0 = 1 \quad \text{when } T > T_{\text{liquidus}},$$

where T_{solidus} and T_{liquidus} are, respectively, solidus temperature (wet and dry solidi is used for the hydrated and dry mantle, respectively) and dry liquidus temperature at a given pressure and rock composition (Table 1). Although melt might accumulate it is likely that before reaching high melt fractions melt collects in channels or dykes and leaves the melting zone (Schmeling, 2006, 2010). Following previous studies, melt ascent is simulated by extracting all melt exceeding locally, a pre-defined melt threshold (e.g., Schmeling, 2010) of $M_{\text{max}} = 4\%$ and a non-extractable amount of melt $M_{\text{min}} = 2\%$ that will remain in the source (e.g., Nikolaeva et al., 2008; Sizova et al., 2010; Gerya and Meilick, 2011). The amount of extracted melt during the evolution of an experiment is tracked by markers. The total amount of melt, M , for every marker takes into account the amount of previously extracted melt and is calculated as

$$M = M_0 - \sum_n M_{\text{ext}},$$

where $\sum_n M_{\text{ext}}$ is the total melt fraction extracted during the previous n extraction episodes. Rocks are considered refractory when the extracted melt fraction is bigger than the standard one (i.e. when $\sum_n M_{\text{ext}} > M_0$). If the total amount of melt exceeds the threshold M_{max} , the melt fraction $M_{\text{ext}} = M - M_{\text{min}}$ is extracted and $\sum_n M_{\text{ext}}$ is updated. It is believed that extracted melts leave the melting zone much faster than rocks deform (Elliott et al., 1997; Hawkesworth et al., 1997). Hence, extracted melts are transmitted instantaneously to emplacement areas in form of plutons and volcanics. It is assumed that 20% of all extracted melts propagate towards the surface forming a volcanic arc above the extraction area, thereby retraining its volume. The remaining 80% emplace at lower levels, forming plutons in the continental crust in areas of highest possible intrusion emplacement rate (i.e., highest possible local crustal divergence rate, $\text{div}_{\text{crust}}$), determined above the melt extraction region by evaluating locally the ratio of the effective melt overpressure to the effective viscosity of the crust:

$$\text{div}_{\text{crust}} = [\text{Py}_{\text{melt}} - g_y \rho_{\text{melt}} (y_{\text{melt}} - y) - \text{Py}] / \eta_y,$$

where Py_{melt} and Py is the pressure at the extraction level y_{melt} and at the current level y , respectively, g_y is the gravitational acceleration in y -direction [m/sek^2], ρ_{melt} is the melt density and η_y is the effective local crustal viscosity at the current level y . Extracted melts are thus emplaced at the level y where the computed possible crustal divergence rate $\text{div}_{\text{crust}}$ is highest. Effects of matrix compaction in the melt extraction area and crustal divergence in the melt emplacement area are taken into account in the compressible continuity equation (e.g., Gerya and Yuen, 2007) that provides correct coupling between local and global flow fields.

2.4. Rheology

The effective creep viscosities of rocks are defined as a function of temperature and stress by experimentally determined flow laws. The viscosity for dislocation creep is defined as follows (Ranalli, 1995):

$$\eta_{\text{creep}} = (\dot{\epsilon}_{\text{II}})^{(1-n)/n} / (A_D)^{1/n} \exp(E/nRT),$$

where $\dot{\epsilon}_{\text{II}} = (1/2 \dot{\epsilon}_{ij} \dot{\epsilon}_{ij})^{1/2}$ is the second invariant of the strain rate tensor. A_D (pre-exponential factor), E (activation energy), n (creep exponent) are experimentally determined flow law parameters and R is the gas constant.

Despite its importance in relation to arc magmatism, the extent, mechanisms and rheological effects of fluid flow and melt percolation are a matter of debate (Weertman, 1971; Clemens and Mawer, 1992; Scambelluri and Philipott, 2001; McKenzie, 1984; Connolly and Podladchikov, 1998; Spiegelman and Kenyon, 1992; Daines

and Kohlstedt, 1994; Stevenson, 1989; Holtzman et al., 2003). At shallow subduction levels, expulsion of large volumes of connate water affects the thermal and rheological evolution of the accretionary prism (e.g., Peacock, 1990). The extent to which fluids affect the rheological strength of the accretionary prism is strongly dependent on the pore fluid pressure (Davies, 1983) that varies according to the nature (coarse terrigenous sedimentation versus finer pelagic sedimentation) and history (fast and slow sedimentation) of the rock column considered (Le Pichon et al., 1993). At greater depth mineral dehydration reactions release water that may alter the bulk composition of the overlying mantle and trigger partial melting (e.g., Tatsumi and Eggins, 1995; Iwamori, 1998). Fluid/melt transfer under arcs may not only alter the bulk composition of the overlying mantle but also its rheological strength. It is well established that the presence of water results in significant weakening of mantle rocks and minerals (Chopra and Paterson, 1984; Mackwell et al., 1985; Karato et al., 1986; Hirth and Kohlstedt, 1996). Similarly, melts have a large effect on the effective viscosity and strength of partially molten rocks (e.g., Kohlstedt and Zimmerman, 1996; Holtzman and Kohlstedt, 2007). The extent to which the rheology of (subducted, mantle) rocks may be affected by percolating melts and fluids is largely uncertain and depends on the dominating physical mechanism of fluid and/or melt flow (diffusion, percolation, reactive flow, etc.) as well as on the physical properties of rocks at depths (such as permeability, porosity, composition etc.). To account for these complex fluid/melt weakening effects to a first order we use a simple parameterized approach (e.g., Gerya and Meilick, 2011). The Mohr–Coulomb yield criterion is implemented which limits the creep viscosity, altogether yielding an effective visco-plastic rheology.

$$\eta_{\text{creep}} \leq \sigma_{\text{yield}} / 2 \dot{\epsilon}_{\text{II}}, \quad \sigma_{\text{yield}} = c + P \sin(\varphi), \\ \sin(\varphi) = \sin(\varphi_{\text{dry}}) \lambda_{\text{fluid}}, \quad \lambda_{\text{fluid}} = 1 - P_{\text{total}} / P_{\text{total}}.$$

The local plastic strength of a rock depends on the mean stress, $P_{\text{total}} = P$ (dynamic pressure), the cohesion, c , which is the strength at $P = 0$, and on the effective internal friction angle, φ , which is calculated from the friction angle of dry rocks, φ_{dry} (for values of c and $\sin(\varphi_{\text{dry}})$ see Table 1), and the pore fluid pressure factor λ_{fluid} . This factor is interpreted as $\lambda_{\text{fluid}} = 1 - P_{\text{fluid}} / P_{\text{total}}$; the pore fluid pressure P_{fluid} reduces the yield strength σ_{yield} of fluid-containing porous or fractured rock. The smaller the pore fluid pressure factor, the larger the weakening effect.

The weakening effect of ascending melts is implemented in a similar manner. Extraction of melt decreases the yield strength σ_{yield} of rocks in the column between the area of the melt generation and emplacement, according to a prescribed melt pressure factor:

$$\lambda_{\text{melt}} = 1 - P_{\text{melt}} / P_{\text{total}}.$$

According to our rheological model major parameters affecting effective viscosity of rocks at relatively cold temperatures are weakening effects of fluids and melts. On the other hand, temperature- and stress-dependences of viscosity are dominant rheological factors for hot rocks. 10^{17} and 10^{25} Pas are the lower and upper cut-off values for viscosity of all types of rocks in our numerical experiments.

2.5. Computational strategy

The model is based on the I2VIS code (Gerya and Yuen, 2003) using conservative finite differences and a non-diffusive marker in cell technique to simulate multiphase flow. The governing conservation equations of mass, momentum and energy and the constitutive relationships between stress and strain-rate (needed in the creeping flow regime) are solved using an irregularly-spaced

staggered grid in Eulerian configuration. Conservation of mass is described by the Lagrangian continuity equation for a compressible fluid. Interpolation between markers and nodes is solved by using a distance dependent bilinear averaging scheme (Gerya and Yuen, 2003). Thus markers located closer to a node have a higher statistical weight.

2.6. Magma terminology

Along this paper, we use the following terms to refer to the distinct magma types generated in the models. We call dacite to melts generated by partial melting of basalts and gabbros that form part of the subducting oceanic slab. These dacitic magmas can reach the surface in the form of dacitic or adakitic primary magmas or, be emplaced as silicic trondhjemitic and tonalite plutons in the continental crust. Also, these dacitic melts may percolate the mantle wedge contributing to metasomatism and fertilization of peridotite. We call granite to melts generated by partial melting of sediments and granodiorite to melts generated within composite plumes formed of subduction mélanges. The term basaltic is used for melts generated by partial melting of the wet peridotite. In spite of being widely accepted, we avoid the use of the term adakite to refer to basalt or gabbro partial melts because adakite is a name restricted for dacitic rocks with a particular geochemical signature related to garnet stability (Moyen, 2009) and, thus, to the prevailing PT conditions of magma generation. The term dacite is more general and informative about major element composition and source composition with independence of pressure and temperature.

3. Results

Here we present a detailed study of crustal growth and evolution of an oceanic-continental subduction process. A key aspect of this study concerns intrusive and extrusive magmatic addition in relation to different geodynamic settings. In contrast to the previous study by Gerya and Meilick (2011) the dynamics of crustal growth have been studied over a range of strong to intermediate fluid and melt related weakening effects ($\lambda_{\text{fluid}} = 0.001\text{--}0.2$; $\lambda_{\text{fluid}} = 0.0\text{--}0.5$; Table 2, Fig. 2). The results of this study as a function of the parameter space are displayed in Fig. 3. This range does not include strongly compressional, ablative subduction regimes (Gerya and Meilick, 2011) with an extreme degree of plate coupling, which may not be relevant for typical active margins (e.g., Sobolev and Babeyko, 2005). For the sake of simplicity, we also do not discriminate between different compressional arc regimes suggested by Gerya and Meilick (2011) since they produce similar magmatic outputs. Consequently, we have investigated three distinct modes of crustal growth:

- (i) Stable arcs characterized by flattened intrusions in the lower crust derived by partial melting of the oceanic crust (basalts, gabbros) and hydrated mantle (wet peridotite).
- (ii) Compressional arcs ascribed to partial melting of slab components (basalts, gabbros, sediments) that lead to plume formation with flattened intrusions in the lower crust and plume emplacement in the upper crust.
- (iii) Extensional arcs associated with backarc spreading and ocean floor development.

Applying a wet olivine rheology (Ranalli, 1995) for the mantle reduces the parameter space to only two distinct modes of crustal growth: compressional and extensional arcs (Table 2, Nos.: 21–23). Below we describe details of crustal growth processes for these three geodynamic regimes.

3.1. Stable arc settings

Our study reveals stable subduction settings if moderate fluid ($\lambda_{\text{fluid}} = 0.01$) and melt weakening ($\lambda_{\text{melt}} = 0.2\text{--}0.5$; reference model, Table 2, No.: 10) is applied. Shortly after subduction initiation (<5 Myrs) the large thermal contrast between the mantle and the leading edge of the slab induces partial melting in the slab nose (Fig. 4) This leads to elevated magmatic addition rates of ($35 \text{ km}^3/\text{km}/\text{Myrs}$) (Fig. 5). Within the next 20 Myrs the thermal contrast between the slab and the mantle remains in a transitional state allowing for partial melting of the oceanic crust, before reaching a thermal equilibrium. Dacitic melts may form and move upwards until they finally form trondhjemitites in the lower crust or dacites at the surface (Fig. 4). Magmatic addition rates decline to typical values of $10 \text{ km}^3/\text{km}/\text{Myrs}$ as the thermal contrast is balanced out (Fig. 5). In the course of subduction, water is expelled due to compaction or as a result of (metamorphic) dehydration reactions. Aqueous fluids percolating from the slab into the mantle wedge may form a serpentinized wedge-like channel at shallow plate interfaces (<130 km), where subducted sediments and oceanic crust intermix. Hence, a tectonic rock mélange is formed. At asthenospheric depth (>100 km) progressive hydration of the slab induces partial melting of wet peridotite. Mafic melts are generated and emplacement in form of flattened intrusions in the lower crust and extrusive volcanics (Fig. 4). Thus volcanic and plutonic rocks are formed, by partial melting of the subducted crustal lithologies (basalts, gabbros, sediments) and mantle components (wet peridotite) with spatial and temporal variations (Fig. 5). The continental crust grows.

Stable subduction zones are characterized by large growing accretionary wedges, which can be divided into two parts: a plug in the retro-wedge next to the continental margin and a pro-wedge, where material is accreted in form of stacked nappes (Fig. 4). Most of the incoming sediments are scrapped off in the course of subduction and piled into nappes at the front of the accretion wedge leading to trench retreat (Fig. 6a). However some of the incoming sediments can also bypass the accretionary wedge as a result of sediment subduction or sediment erosion. Beneath the continental crust, basal erosion is facilitated by sufficiently strong coupling of the plates (Fig. 4). Serpentinized mantle mixed with basalts, gabbros and sediments from the subducting slab, moves upward and removes crustal material from the upper crust and accretionary prism.

3.2. Compressional arcs with plume development

Compressional arcs associated with plume development can be observed in experiments with reduced fluid weakening ($\lambda_{\text{fluid}} \geq 0.1$; reference model, Table 2, No.:13). At first crust formation is attributed to partial melting of the slab nose, forming dacitic melts. Intrusive trondhjemitites and extrusive dacites may form (Fig. 7), similar to stable arcs. In the course of subduction strong coupling of the plates leads to back-arc compression (Fig. 6b) and enhances sediment subduction. Localization and partial melting of sediments and basalts atop the slab results in an extended rock mélange formation, thick enough to trigger upwellings followed by plume development. Favorable conditions for partial melting of slab components are reached at asthenospheric depth, where partial melting of the rock mélange produces thermal-chemical sedimentary plumes (Fig. 7). Melts extracted from partially molten rocks (Fig. 8), which are formed both atop the slab and inside the plumes, are emplaced in form of extrusive volcanics (dacites, rhyolites) and intrusive plutons (trondhjemitites, granites, granodiorites). Once a critical amount of buoyant mass is reached these plumes ascend from the slab and may intrude into the crust where they finally crystallize as silicic intrusions (batholiths)

Table 2
Description of numerical experiments.

No.	λ_{fluid}	λ_{melt}	v_{sub} [cm/year]	v_{op}	Mantle [Flow law/Pas]	Serpentine	Geodynamic Regime
1	0.001	0	5	0	Dry olivine	10^{18}	Extensional arc
2	0.001	0.001	5	0	Dry olivine	10^{18}	Extensional arc
3	0.001	0.01	5	0	Dry olivine	10^{18}	Extensional arc
4	0.001	0.2	5	0	Dry olivine	10^{18}	Extensional arc
5	0.001	0.5	5	0	Dry olivine	10^{18}	Extensional arc
6	0.01	0	5	0	Dry olivine	10^{18}	Extensional arc ^a
7	0.01	0.001	5	0	Dry olivine	10^{18}	Extensional arc
8	0.01	0.01	5	0	Dry olivine	10^{18}	Extensional arc
9	0.01	0.2	5	0	Dry olivine	10^{18}	Stable arc
10	0.01	0.5	5	0	Dry olivine	10^{18}	Stable arc ^a
11	0.1	0	5	0	Dry olivine	10^{18}	Compressional arc
12	0.1	0.001	5	0	Dry olivine	10^{18}	Compressional arc
13	0.1	0.01	5	0	Dry olivine	10^{18}	Compressional arc ^a
14	0.1	0.2	5	0	Dry olivine	10^{18}	Compressional arc
15	0.1	0.5	5	0	Dry olivine	10^{18}	Compressional arc
16	0.2	0	5	0	Dry olivine	10^{18}	Compressional arc
17	0.2	0.001	5	0	Dry olivine	10^{18}	Compressional arc
18	0.2	0.01	5	0	Dry olivine	10^{18}	Compressional arc
19	0.2	0.2	5	0	Dry olivine	10^{18}	Compressional arc
20	0.2	0.5	5	0	Dry olivine	10^{18}	Compressional arc
21	0.01	0	5	0	wet olivine	10^{18}	Compressional arc
22	0.01	0.5	5	0	wet olivine	10^{18}	Compressional arc
23	0.1	0.01	5	0	wet olivine	10^{18}	Extensional arc
24	0.01	0	5	2	Dry olivine	10^{18}	Compressional arc
25	0.01	0.5	5	2	Dry olivine	10^{18}	Compressional arc
26	0.1	0.01	5	2	Dry olivine	10^{18}	Compressional arc
27	0.01	0	5	4	Dry olivine	10^{18}	Compressional arc
28	0.01	0.5	5	4	Dry olivine	10^{18}	Compressional arc
29	0.1	0.01	5	4	Dry olivine	10^{18}	Compressional arc
30	0.1	0.01	5	0.5	Dry olivine	Wet olivine	Compressional arc
31	0.1	0.01	5	1	Dry olivine	Wet olivine	Compressional arc
32	0.1	0.01	5	2	Dry olivine	Wet olivine	Compressional arc
33	0.1	0.01	6	4	Dry olivine	Wet olivine	Compressional arc
34	0.001	0.001	3	0	Dry olivine	Wet olivine	Extensional arc
35	0.001	0.01	3	0	Dry olivine	Wet olivine	Extensional arc
36	0.001	0.2	3	0	Dry olivine	Wet olivine	Stable arc
37	0.01	0.001	3	0	Dry olivine	Wet olivine	Extensional arc
38	0.01	0.01	3	0	Dry olivine	Wet olivine	Extensional arc
39	0.01	0.2	3	0	Dry olivine	Wet olivine	Stable arc
40	0.1	0.001	3	0	Dry olivine	Wet olivine	Compressional arc
41	0.1	0.01	3	0	Dry olivine	Wet olivine	Compressional arc
42	0.1	0.2	3	0	Dry olivine	Wet olivine	Compressional arc
43	0.2	0.001	3	0	Dry olivine	Wet olivine	Compressional arc
44	0.2	0.01	3	0	Dry olivine	Wet olivine	Compressional arc
45	0.2	0.2	3	0	Dry olivine	Wet olivine	Compressional arc
46	0.001	0.001	3	0.5	Dry olivine	Wet olivine	Extensional arc
47	0.001	0.01	3	0.5	Dry olivine	Wet olivine	Extensional arc
48	0.001	0.2	3	0.5	Dry olivine	Wet olivine	Stable arc
49	0.01	0.001	3	0.5	Dry olivine	Wet olivine	Extensional arc
50	0.01	0.01	3	0.5	Dry olivine	Wet olivine	Extensional arc
51	0.01	0.2	3	0.5	Dry olivine	Wet olivine	Stable arc
52	0.1	0.001	3	0.5	Dry olivine	Wet olivine	Compressional arc
53	0.1	0.01	3	0.5	Dry olivine	Wet olivine	Compressional arc
54	0.1	0.2	3	0.5	Dry olivine	Wet olivine	Compressional arc
55	0.2	0.001	3	0.5	Dry olivine	Wet olivine	Compressional arc
56	0.2	0.01	3	0.5	Dry olivine	Wet olivine	Compressional arc
57	0.2	0.2	3	0.5	Dry olivine	Wet olivine	Compressional arc
58	0.001	0.001	3	1	Dry olivine	Wet olivine	Stable arc
59	0.001	0.01	3	1	Dry olivine	Wet olivine	Stable arc
60	0.001	0.2	3	1	Dry olivine	Wet olivine	Stable arc
61	0.01	0.001	3	1	Dry olivine	Wet olivine	Stable arc
62	0.01	0.01	3	1	Dry olivine	Wet olivine	Stable arc
63	0.01	0.2	3	1	Dry olivine	Wet olivine	Stable arc
64	0.1	0.001	3	1	Dry olivine	Wet olivine	Stable arc
65	0.1	0.01	3	1	Dry olivine	Wet olivine	Stable arc
66	0.1	0.2	3	1	Dry olivine	Wet olivine	Stable arc
67	0.2	0.001	3	1	Dry olivine	Wet olivine	Compressional arc
68	0.2	0.01	3	1	Dry olivine	Wet olivine	Compressional arc
69	0.2	0.2	3	1	Dry olivine	Wet olivine	Compressional arc
70	0.001	0.001	3	2	Dry olivine	Wet olivine	Stable arc
71	0.001	0.01	3	2	Dry olivine	Wet olivine	Stable arc
72	0.001	0.2	3	2	Dry olivine	Wet olivine	Stable arc
73	0.01	0.001	3	2	Dry olivine	Wet olivine	Stable arc

Fig. 10

Fig. 4

Fig. 7

Table 2 (continued)

No.	λ_{fluid}	λ_{melt}	v_{sub} [cm/year]	v_{op}	Mantle [Flow law/Pas]	Serpentine	Geodynamic Regime
74	0.01	0.01	3	2	Dry olivine	Wet olivine	Stable arc
75	0.01	0.2	3	2	Dry olivine	Wet olivine	Stable arc
76	0.1	0.001	3	2	Dry olivine	Wet olivine	Stable arc
77	0.1	0.01	3	2	Dry olivine	Wet olivine	Compressional arc
78	0.1	0.2	3	2	Dry olivine	Wet olivine	Stable arc
79	0.2	0.001	3	2	Dry olivine	Wet olivine	Compressional arc
80	0.2	0.01	3	2	Dry olivine	Wet olivine	Stable arc
81	0.2	0.2	3	2	Dry olivine	Wet olivine	Compressional arc

λ_{fluid} pore fluid pressure factor.

λ_{melt} melt pressure factor.

v_{sub} velocity of the subducting plate [cm/year].

v_{op} trenchward motion of the overriding plate [cm/year].

Dry olivine Ranalli, 1995 (see Table 1 for details).

Wet olivine Ranalli, 1995 (see Table 1 for details).

10^{18} [Pas] constant viscosity.

Nos.: 1–20 see Fig. 2.

Nos.: 34–81 see Fig. 12.

^a Reference model described in text.

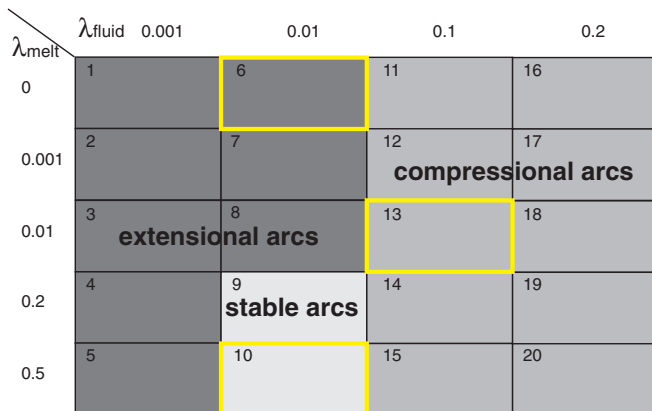


Fig. 2. Parameter space showing the explored range of variations of fluid- (λ_{fluid}) and melt-related (λ_{melt}) weakening effects. Small values of λ_{fluid} and λ_{melt} correspond to strong weakening. Models are classified into three groups: stable arcs, compressional arcs and extensional arcs. Respective reference models are marked in yellow. (For interpretation of the references to colour in this figure legend, the reader is referred to the web version of this article.)

(Fig. 7) or underplate the lithosphere (Fig. 9). Enhanced melt weakening weakens the continental lithosphere and enables plume emplacement, reduced weakening leads to underplating plumes (Table 2, Nos.: 14, 15, 19, 20). In cases where plume emplacement occurs, local extension and slab retreat are observed (Fig. 6b).

Reduced weakening by fluids strengthens the sediments atop the slab allowing for sediment subduction. Most of the incoming sediments bypass the accretionary wedge and only small to medium sized prisms are formed. Local extension due to plume emplacement and material uplift next to the continental margin causes a flexure of the continental plate forming a forearc basin (Figs. 6b and 7).

3.3. Extensional arcs

Extensional arcs develop in subduction zones with strong weakening by fluids ($\lambda_{\text{fluid}} = 0.01$; $\lambda_{\text{fluid}} = 0.01$ and $\lambda_{\text{melt}} \leq 0.2$; reference model, Table 2, No.: 6). Shortly after subduction initiation hydration of the oceanic crust triggers partial melting. Melts derived by partial melting of the slab, move upward forming a magmatic arc at the surface and flattened intrusions in the lower crust until

they finally solidify (Fig. 10). Magmatic addition rates are relatively low, as shown in Fig. 11. The propagation of melts weakens the lithosphere. In addition the emplacement of newly produced crust leads to extension within the lithosphere followed by lithospheric necking (Fig. 10). The backward motion of the subduction zone relative to the motion of the plate leads to thinning of the overriding plate. Thus hot and dry asthenosphere rises into the neck as the slab retreats, triggering decompression melting of dry peridotite. The onset of dry decompression melting associates with an increase in the thermal contrast between the slab and the mantle and partial melting of the subducting oceanic crust. After approximately 15 Myrs a backarc spreading center is formed and crustal growth rates rise from about $40 \text{ km}^3/\text{km}/\text{Myrs}$ to $80 \text{ km}^3/\text{km}/\text{Myrs}$. New MORB like crust is produced of mainly basaltic composition (Fig. 11) at a spreading rate of 0.1–0.2 cm/year (Fig. 6c). Magmatic addition rates may exceed $100 \text{ km}^3/\text{km}/\text{Myrs}$. The thickness of the new MORB-like crust varies from 5 km around the spreading center to 8–10 km toward the edges. After 20 Myrs the comparably dense material subsides slightly and the MORB-like crust is flooded (Fig. 10).

Subduction of the oceanic plate leads to frontal accretion of the incoming sediments forming stacked nappes in the pro-wedge and a plug in the retro-wedge with minor sediment subduction, similar to a stable arc setting (Fig. 6c).

3.4. Influences of overriding plate velocity

We have tested the effect of different overriding plate velocities (Table 2, Nos.: 24–81; Fig. 12). In agreement with previous studies, we found that the trenchward motion of the upper plate has a major influence on the coupling of the plates (Sobolev and Babeyko, 2005), backarc stresses (Schellart, 2008), slab dip (e.g., van Hunen et al., 2000, 2002) and, consequently on the crustal growth regime. The radius of the slab curvature was calculated using three points measured at 30, 70 and 130 km depth (Fig. 13). Small radii correspond to strongly curved, steeply dipping slabs, large radii are characteristic for gently bended, shallow dipping slabs.

Flattening of the subduction dip with time is a common scenario of all encountered experiments. The degree of this decrease and the radius of the slab curvature at a given time depend on the velocity of the overriding plate and the total convergence rate. Enhanced and reduced velocities result in shallow and steep dipping slabs, respectively. The faster the overriding plate moves (toward the trench), the shallower the angle of subduction that is

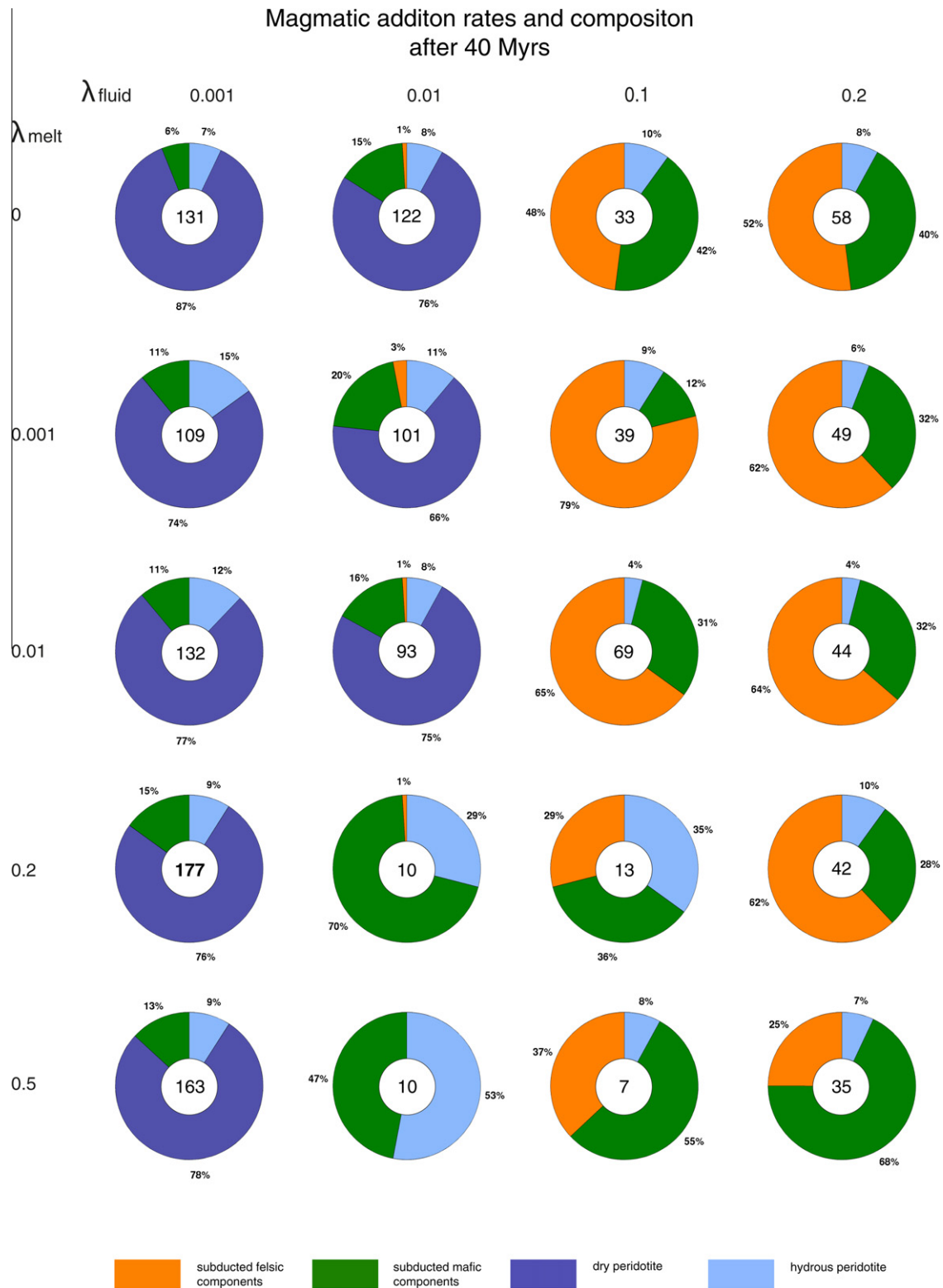


Fig. 3. Magmatic addition rates ($[\text{km}^3/\text{km}/\text{Myrs}]$, displayed in circles) and compositions (pie chart) of all encountered experiments after 40 Myrs (Table 2, Nos.: 1–20). Rates of crust formation are highest for extensional arcs where approximately 75% of the newly formed crust is formed by decompression melting of dry peridotite. Most of the crust formed in stable arc settings is derived by partial melting of the oceanic crust and hydrated mantle (flux melting). Magmatic addition rates are low ($10 \text{ km}^3/\text{km}/\text{Myrs}$). In compressional arcs, most of the newly formed crust is derived by partial melting of sediments and basalts atop the slab and inside the plumes (up to 96%). Partial melting of the hydrous peridotite becomes more important for underplating plumes (up to 35%).

in accordance with previous studies (e.g., van Hunen et al., 2000). Variations of the upper plate motion have moreover an influence on the geodynamic regime of crustal growth. An enhanced upper

plate motion (Fig. 12) or increasing convergence rate increases the sedimentation drag, reduces accretion and promotes back arcs stresses. Extensional arcs are not achieved for enhanced upper

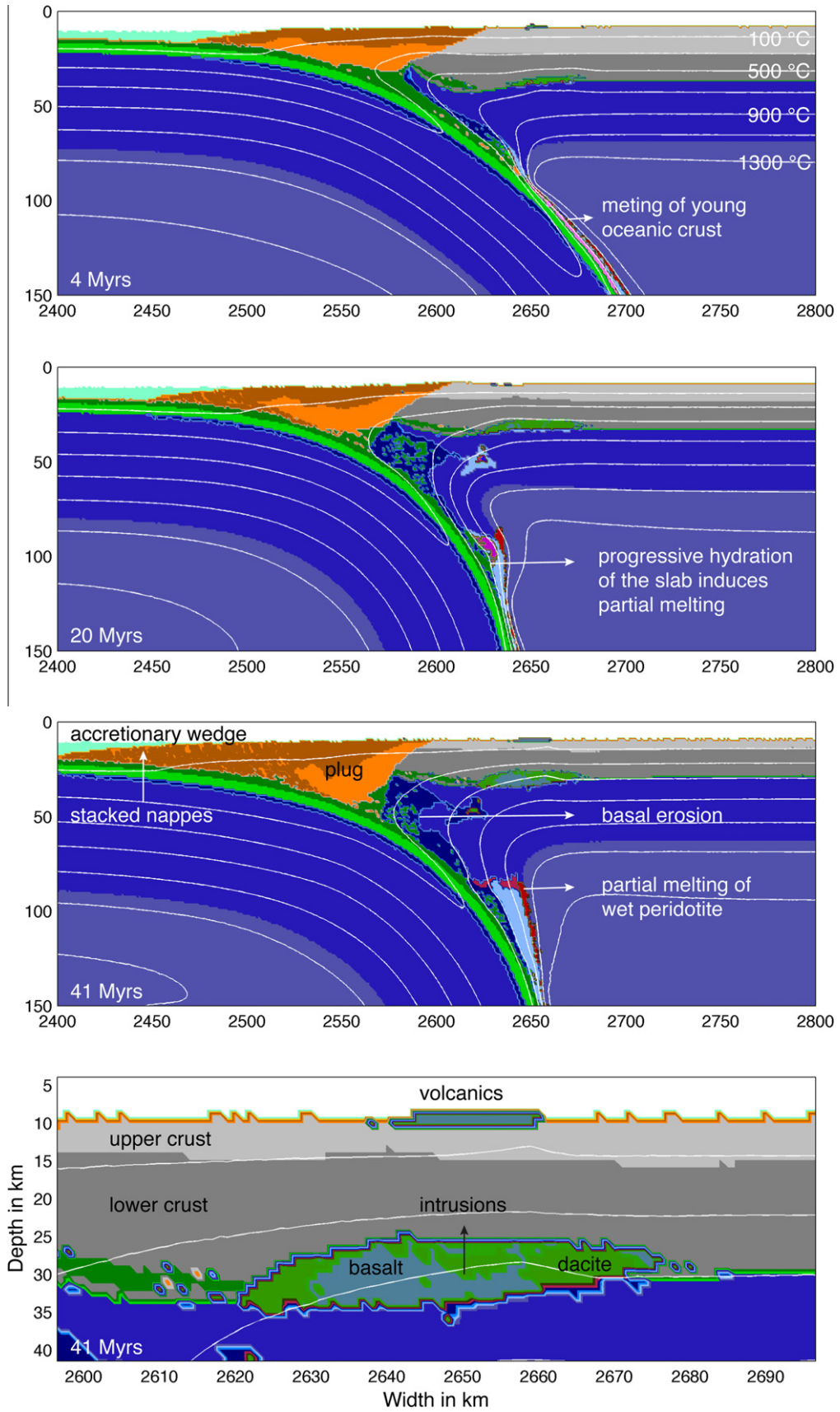


Fig. 4. Evolution of the reference model for stable subduction arcs ($\lambda_{\text{fluid}} = 0.001$, $\lambda_{\text{melt}} = 0.5$; Table 2, No.: 10). No backarc spreading is developed and no sedimentary plumes are formed. Volcanics at the surface and flattened intrusions in the lower crust are formed, due to partial melting of slab and mantle components, resulting in dacitic and basaltic intrusion, respectively. Frontal accretion of incoming sediments forms a laterally growing sedimentary wedge.

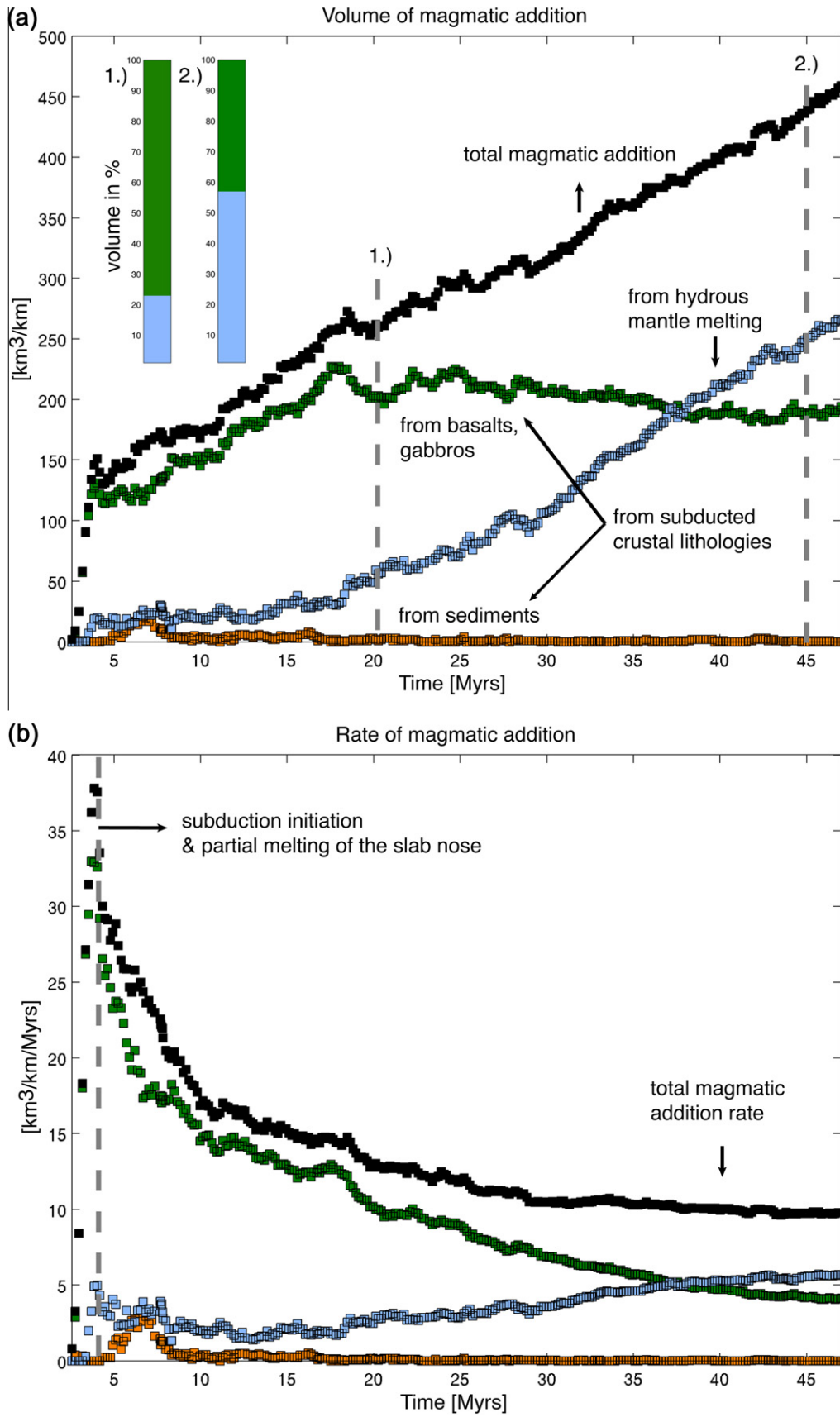


Fig. 5. Dynamics of crustal growth of stable arc settings (Table 2, No.: 10). Lithological structure of newly formed crust (a) and magmatic addition rates of magmas derived from different sites of production (b). At first crustal growth is attributed to partial melting of the young slab. Subsequently hydration of the mantle induces partial melting of wet peridotite. Crustal growth rates are low.

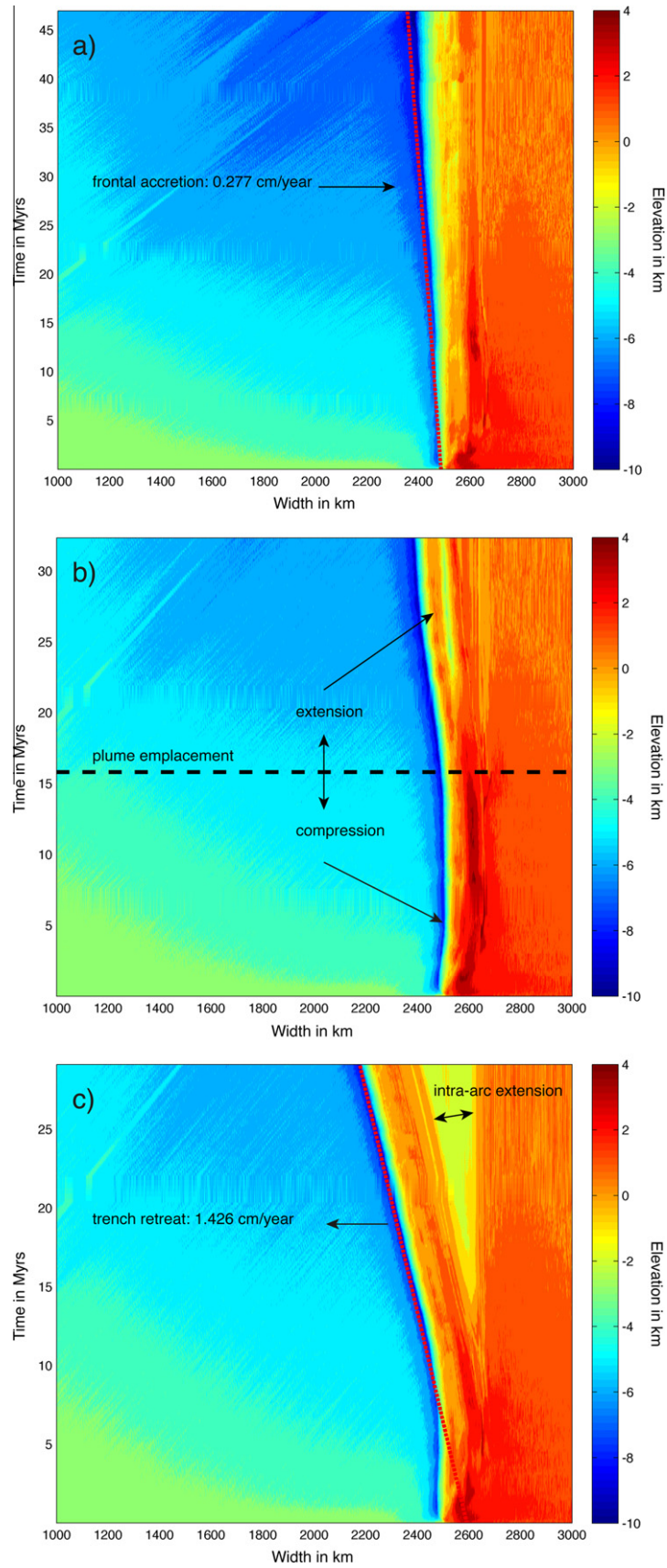


Fig. 6. Topography evolution of stable (a), compressional (b) and extensional arcs (c). (a) The backward movement of the trench is solely attributed to frontal accretion of sediments, scrapped of the subducting slab. The trench retreats as the sedimentary wedge grows laterally. (b) Strong coupling of the plates promotes compression in the back-arc, followed by local extension due to plume emplacement. (c) Frontal accretion of sediments and back-arc extension lead to trench retreat. Focused back-arc spreading and intra-arc extension are observed.

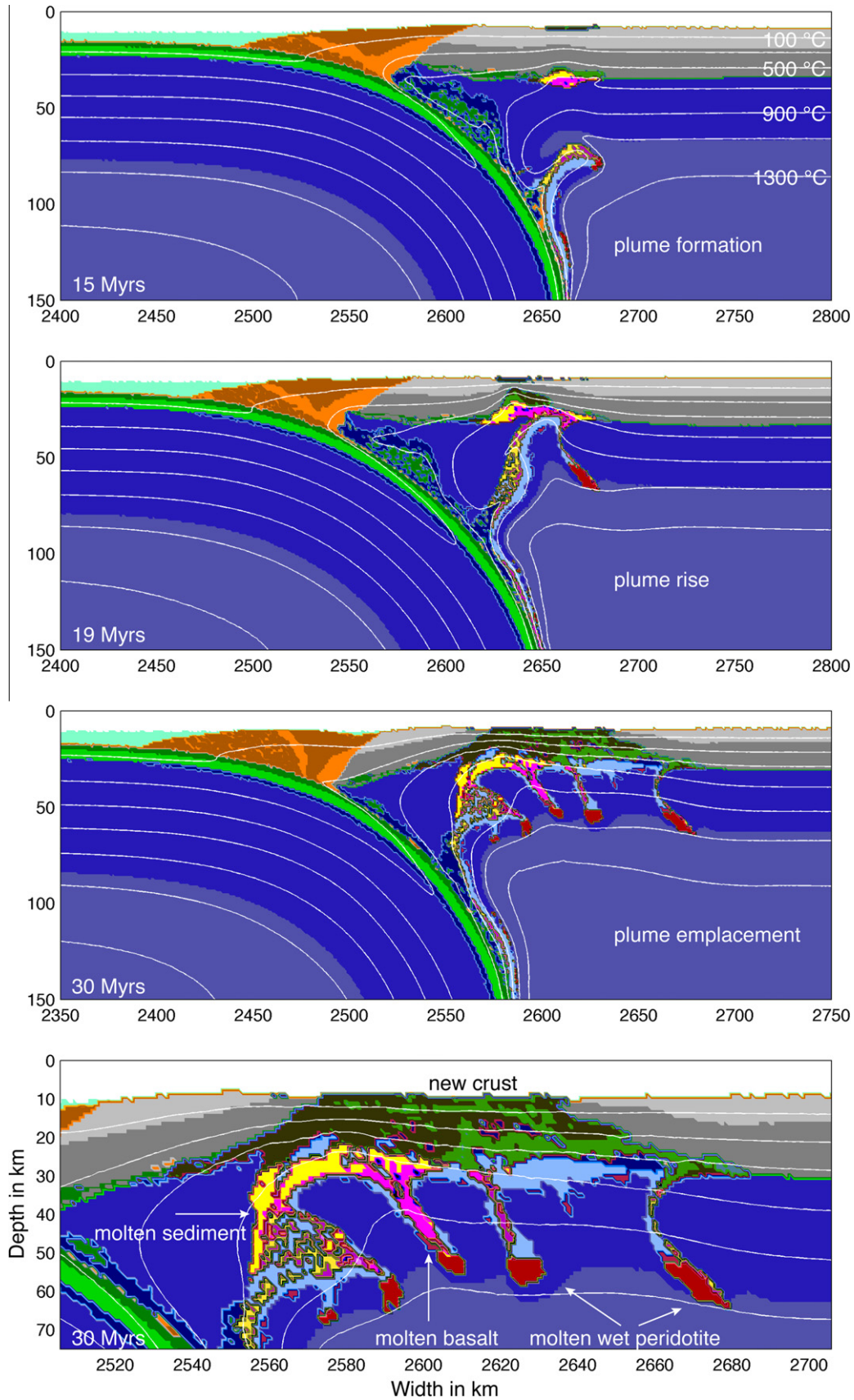


Fig. 7. Development of the reference model for compressional arcs with plume development ($\lambda_{\text{fluid}} = 0.1$, $\lambda_{\text{melt}} = 0.001$; Table 2, No.: 13). No backarc spreading center develops. Hybrid plumes form at asthenospheric depth. Followed by rapid plume rise and further plume development. Magmatic addition is ascribed to plume emplacement and partial melting of mainly slab components located atop the slab, forming flattened intrusions in the lower crust.

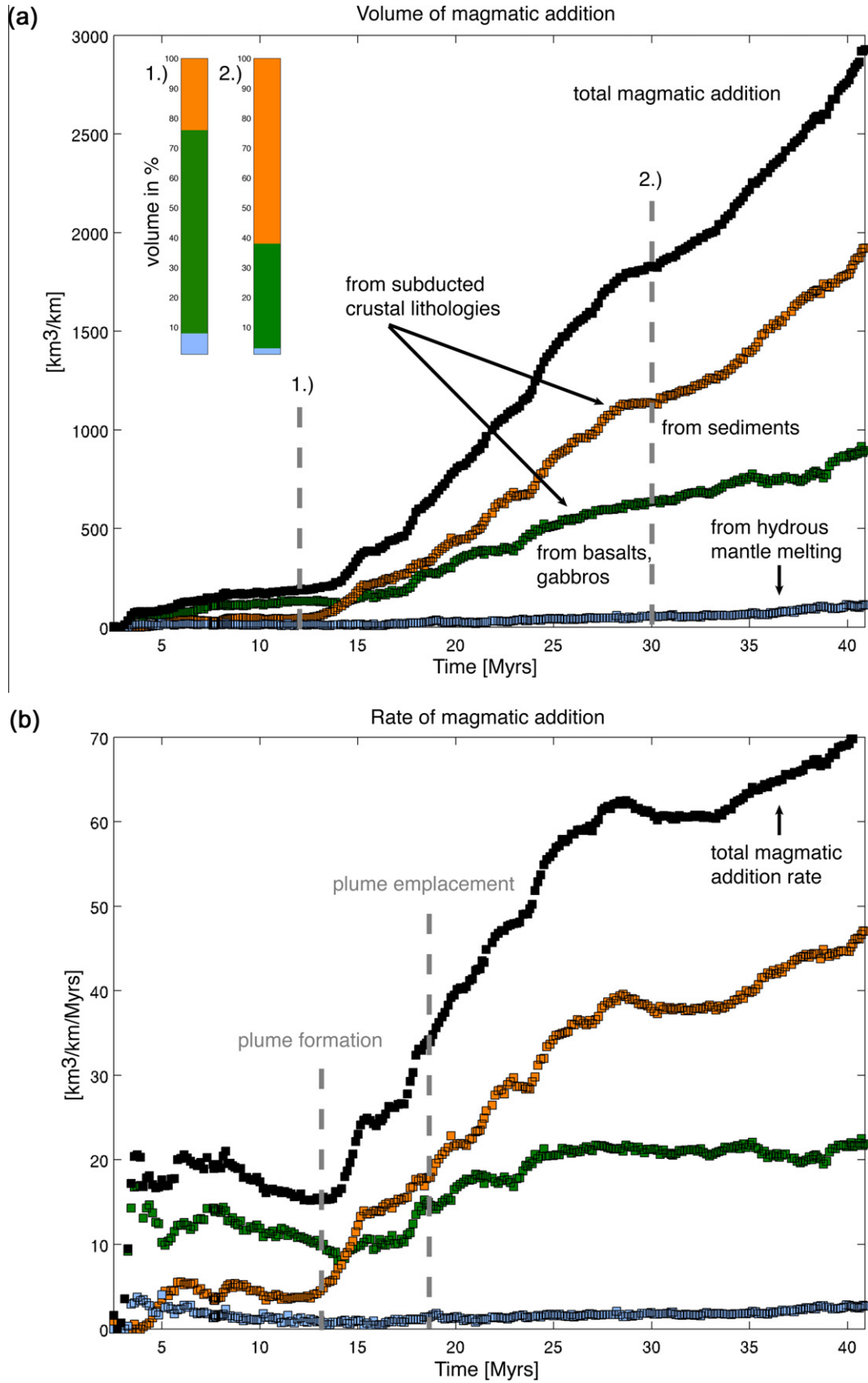


Fig. 8. Dynamics of crustal growth of compressional arc settings (Table 2, No.: 13). Lithological structure of newly formed crust (a) and magmatic addition rates of magmas derived from different sites of production (b). Magmatic addition is mainly attributed to partial melting of sediments and basalts inside the plume and atop the slab. At first magmatic addition rates are low ($20 \text{ km}^3/\text{km}/\text{Myrs}$) but rise rapidly in the course of plume formation and emplacement ($60\text{--}70 \text{ km}^3/\text{km}/\text{Myrs}$).

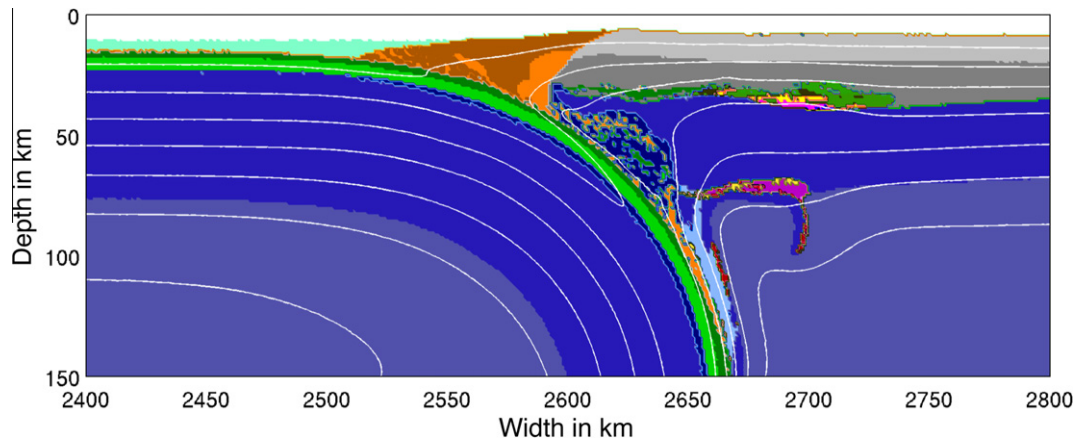


Fig. 9. Underplating plume (Table 2, No.: 14). Reduced fluid and melt weakening ($\lambda_{\text{fluid}} \geq 0.1$, $\lambda_{\text{melt}} \geq 0.2$) result in underplating plumes.

plate velocities and only stable and compressional arcs develop (Fig. 12; Table 2 and 24–81).

4. Discussion

4.1. Magmatic addition rates

Based on our experiments it can be shown that the mode of crustal growth is strongly dependent on the geodynamic regime, namely extension, compression and stable (Fig. 3). The lowest rates of crust formation are found in stable arc settings ($10 \text{ km}^3/\text{km}/\text{Myrs}$, Fig. 3), where magmatic addition is attributed to partial melting of the downgoing oceanic crust and wet peridotite mantle (Fig. 5). The result will be a new mafic crust in which basalts are more abundant than felsic magmas of broadly dacitic to andesitic composition. In compressional arcs, however, the emplacement of hybrid plumes (basalts plus sediments) and partial melts from atop the slab and inside the plume lead to magmatic addition rates of $40\text{--}70 \text{ km}^3/\text{km}/\text{Myrs}$ (Fig. 3), three to seven times higher compared to the stable arc setting (Fig. 8). Extensional arcs associated with new ocean floor development reveal even more elevated crustal growth rates of up to $180 \text{ km}^3/\text{km}/\text{Myrs}$ (Fig. 3). However, these values are at the upper bound because new oceanic crust is included in the computation (magmatic addition rates of natural arc systems do not typically include new oceanic crust formed by decompression melting around backarc spreading centers) (Fig. 11). If products of dry melting are excluded values drop down to $30 \text{ km}^3/\text{km}/\text{Myrs}$. Thus, magmatic addition rates for the three end-member tectonic models vary between 10 and $70 \text{ km}^3/\text{km}/\text{Myrs}$.

Our results are in good agreement with natural observations. Reymer and Schubert (1984) analyzed crustal volumes added to 17 arcs during its active lifespan and calculated growth rates of $20\text{--}40 \text{ km}^3/\text{km}/\text{Myrs}$ per arc length. More recent estimates of the same region are somewhat higher. Tiara et al. (1998) estimated the magmatic addition rate of the Izu-Bonin island arc to be $80 \text{ km}^3/\text{km}/\text{Myrs}$ and similar values ($82 \text{ km}^3/\text{km}/\text{Myrs}$) were obtained for the Aleutian island arcs by Holbrook et al. (1999). In the Atlantic, seismic data from the South Sandwich Island arc gave an arc growth rate of $60 \text{ km}^3/\text{km}/\text{Myrs}$ (Larter et al., 2001). In the study made by Dimalanta et al. (2002) comparison between different growth rates throughout the western Pacific (Aleutians, Northern and Southern Izu-Boni, Marianas, New Hebrides, Tonga) revealed varying magmatic addition rates of $30\text{--}95 \text{ km}^3/\text{km}/\text{Myrs}$. Less data are available for continental margins, where oceanic crust is subducted beneath continental lithosphere. Estimates on

crustal growth rates of cordilleran orogenic systems exhibit cyclic behavior with high flux episodes ($30\text{--}90 \text{ km}^3/\text{km}/\text{Myrs}$) separated by magmatic lulls ($20\text{--}30 \text{ km}^3/\text{km}/\text{Myrs}$) (DeCelles et al., 2009).

4.2. Composition

All regimes display an elevated growth rate (of $35 \text{ km}^3/\text{km}/\text{Myrs}$) soon after subduction initiation ($<5 \text{ Myrs}$) due to partial melting of the slab nose. Because of the large thermal contrast between the mantle and the slab, temperatures at the slab interface may exceed $700 \text{ }^\circ\text{C}$ at depth greater than 80 km , resulting in partial melting. In addition, approximately 20 Myrs are needed to balance out the large thermal contrast as shown for stable arcs. Thus partial melting of the subducting slab occurs simultaneously with dehydration reactions, forming dacitic melts. Consistent with our experiments, dacitic magmas with adakitic signatures found in some volcanic arcs associated to subduction of young oceanic crust, are believed to result from slab melting where temperatures exceed $700 \text{ }^\circ\text{C}$ (Defant and Drummond, 1990; Drummond and Defant, 1990; Sajona et al., 1993; Peacock et al., 1994). For slabs younger than $20\text{--}30 \text{ Myrs}$, Drummond and Defant (1990) envisioned a fertile melting zone at $75\text{--}85 \text{ km}$ depth and $700\text{--}775 \text{ }^\circ\text{C}$, where wet partial melting of the subducting slab occurs concurrently with dehydration reactions (dehydration melting). Ringwood (1989) concluded, that slab derived melts, which are formed at depths ranging from 100 to 300 km , may migrate into the adjacent regions of depleted or refractory peridotite, undergoing hybridization and resulting in the refertilisation of these regions, as it was lately confirmed by laboratory experiments (Prouteau et al., 2001). In general, adakites can be subdivided into two groups, high SiO_2 – adakites (HAS; $\text{SiO}_2 > 60 \text{ wt.}\%$) and low SiO_2 –adakites (LSA; $\text{SiO}_2 < 60 \text{ wt.}\%$) (Martin and Moyen, 2003). The former are considered to represent subducted basaltic-slab melts that have reacted with peridotite during ascent through the mantle wedge, whereas LSA are interpreted to have formed by melting of a peridotitic mantle wedge whose composition has been modified by reaction with felsic melts (Martin et al., 2005). Nevertheless, the composition of these melts may not only be governed by the composition and mineralogy of the source rock, the depth of melting, and the melting reactions, but also by the physical process controlling its migration and segregation (Jackson et al., 2004). After reaching a thermal steady state at the slab interface, crustal growth is attributed to partial melting of the hydrated mantle (Fig. 5). Water expelled from the subducting plate lowers the melting temperature of rocks and causes “flux melting”, which is believed to generate most arc magmas (e.g., Tatsumi, 1986; Iwamori, 1998). Melt inclusions found in arc lavas containing high water contents (as much as 6

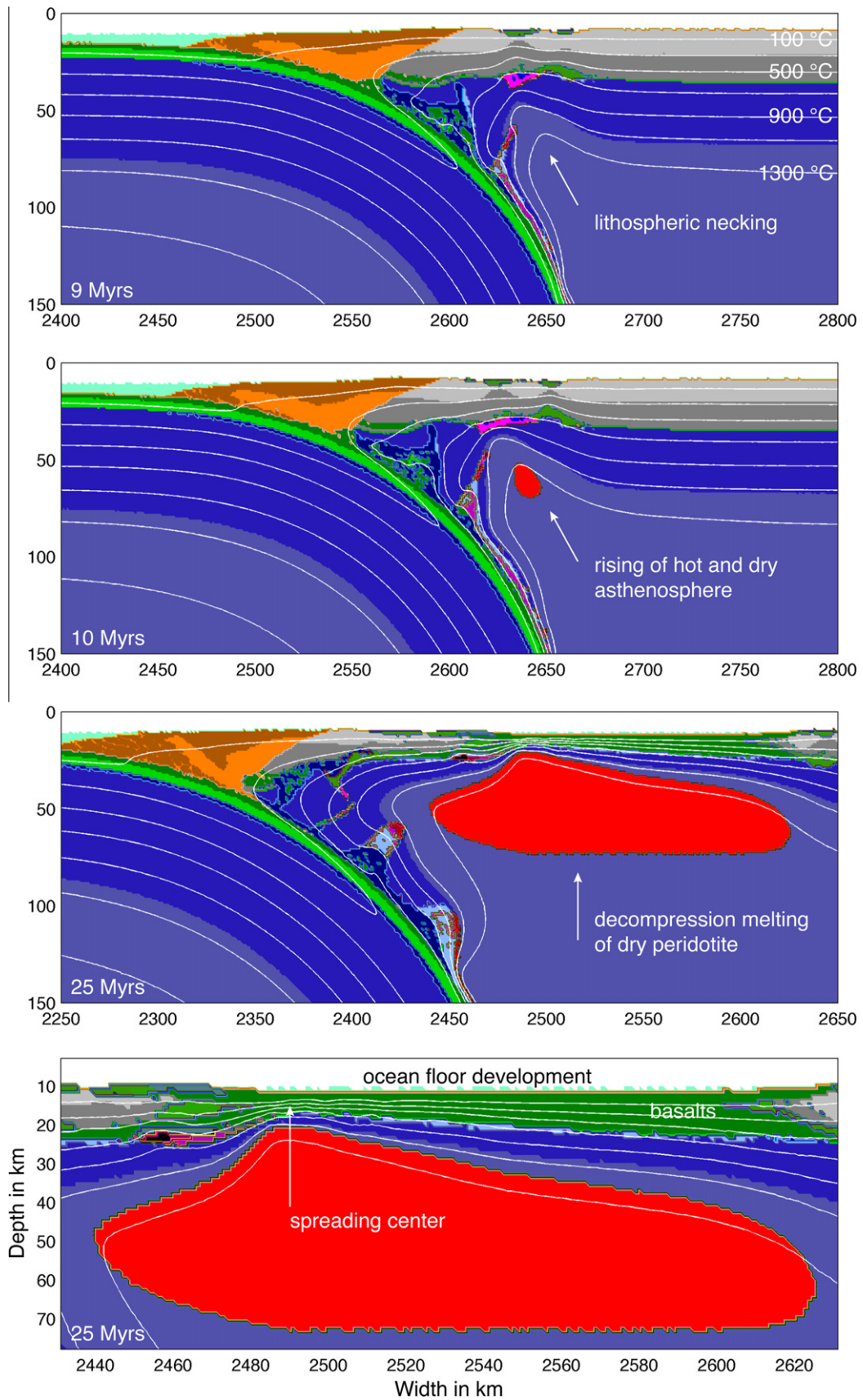


Fig. 10. Development of the reference model for extensional arcs ($\lambda_{\text{fluid}} = 0.001$, $\lambda_{\text{melt}} = 0.001$; Table 2, No.: 6). A focused backarc spreading center develops from intra-arc extension leading to trench retreat. No sedimentary plumes are observed. Early stage crust formation is attributed to partial melting of the slab, forming trondhjemitic intrusions in the lower crust. Followed by extension in the back-arc, enabling decompression melting of dry peridotite and ocean floor development.

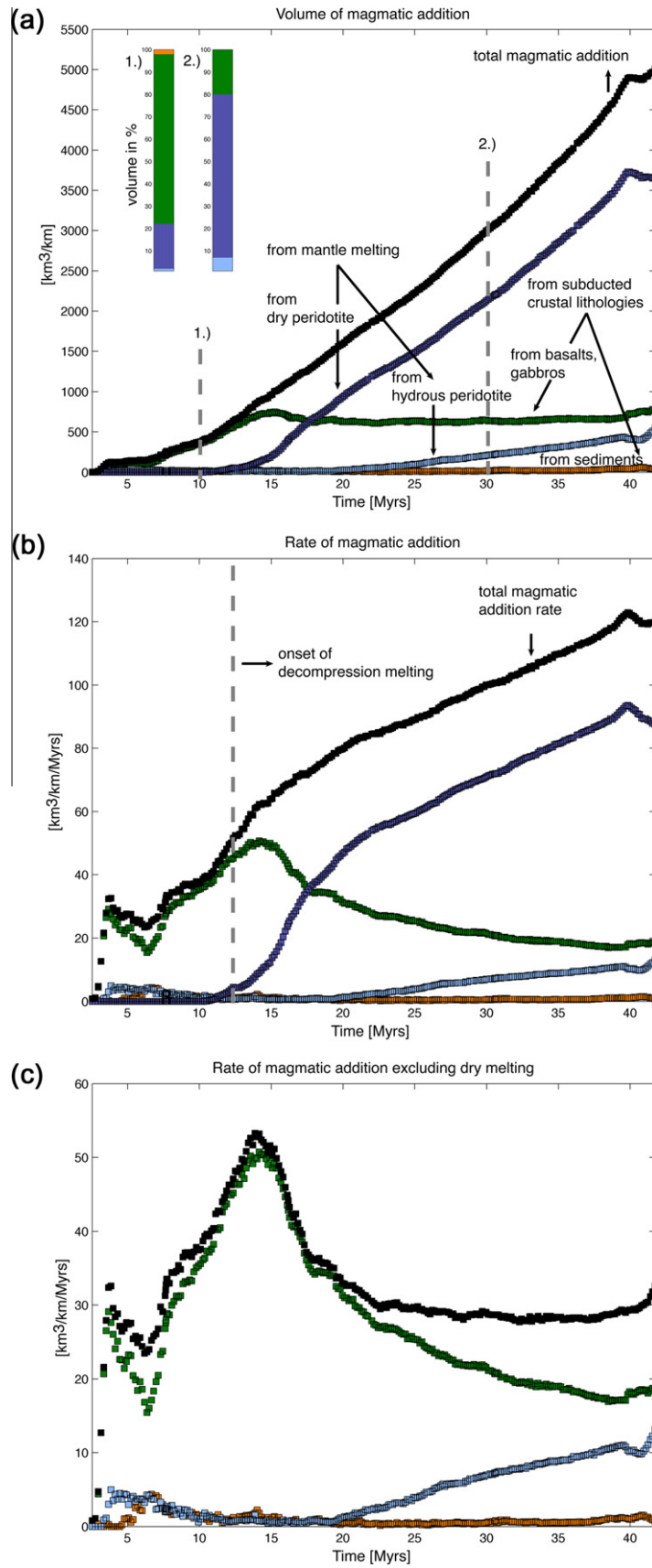


Fig. 11. Dynamics of crustal growth of extensional arc settings (Table 2, No.: 6). Lithological structure of newly formed crust (a) and magmatic addition rates of magmas derived from different sites of production including melts derived by decompression melting (b) and excluding dry mantle melting (c). Back-arc extension leads to extensive decompression melting of dry peridotite. Magmatic addition rates rise to $100 \text{ km}^3/\text{km}/\text{Myrs}$ (b). If dry melting is excluded these values drop to $40\text{--}60 \text{ km}^3/\text{km}/\text{Myrs}$ (c).

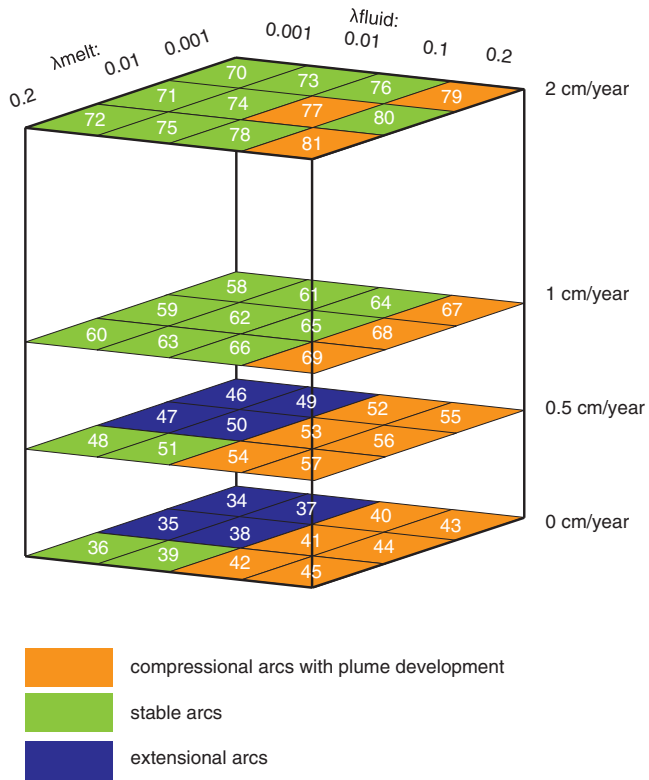


Fig. 12. Parameter space. Rheological weakening effects induced by fluids and melts were tested against a fixed subducting plate velocity (3 cm/year) and varying overriding plate velocities ($v_{op} = 0$ cm/year, $v_{op} = 0.5$ cm/year, $v_{op} = 1$ cm/year, $v_{op} = 2$ cm/year; Table 2: 34–81). The trenchward motion of the upper plate has a major influence on the coupling of the plates. Enhanced upper plate velocities lead to strong coupling of the plates promoting compressional arcs. Extensional arcs do not form for enhanced upper plate velocities.

wt.%) (Sisson and Layne, 1993; Sobolev and Chaussidon, 1996) are consistent with fluids, percolating from the subducting slab into the mantle wedge, inducing melting. This process is ubiquitous in all experiments presented here, where basaltic intrusions are derived by partial melting of wet peridotite. In contrast, mid ocean ridge-basalts (MOR) and ocean island basalts (OIB) are believed to have formed by decompression melting of dry mantle (Langmuir et al., 1992; McKenzie and Bickle, 1988), similar to our experiments of extensional arcs associated with ocean floor development. Although there is some evidence for dry melting beneath arcs related to subduction as shown by Sisson and Bronto (1998), it is unlikely that these rocks make a significant material contribution to average continental crust (Hawkesworth and Kemp, 2006).

However, the continental crust has an andesitic bulk composition, which cannot have been produced by the basaltic magmatism that dominates sites of present day crustal growth (Rudnick, 1995). Basaltic intrusions added to the crust might undergo further assimilation and fractional crystallization leading to the formation of felsic rocks (granodiorites, tonalites) as proposed by some workers (Bigazzi et al., 1986; Macera et al., 1985; Taylor, 1980; Thompson et al., 2002). It is expected that mantle derived magmas fractionate and assimilate progressively so that the latest plutons are the most evolved and most radiogenic. This time-compositional evolution is observed in some Cordilleran batholiths of South America (e.g., the Patagonian batholith, Pankhurst et al., 1999) but only for Sr–Nd isotopes and not for major elements, which remains unmodified in the most evolved plutons as it can be expected in an assimilation process. This model is supported by geological observations of mafic rocks associated with granitoids (Blundy and Sparks, 1992; Ulmer et al., 1985). However, this model does not account for the

large Cordilleran batholiths generated during Mesozoic times along the American active continental margin from Alaska to Antarctica (Castro et al., 2010). In compressional arcs the emplacement of hybrid plumes adds additional material to the continental crust. Partially molten rock mélanges accumulate at asthenospheric depth forming plumes, which rise through the mantle prior to emplacement. These observations are supported by experiments related to the production of silicic plutons from subducted rock mélanges at sublithospheric depths (Castro and Gerya, 2008; Castro et al., 2010). Partial melting of rock mélanges composed of sediments (Bt-rich metagreywacke) and basalts (MORB) produces liquids of granodiorite to tonalite composition (Castro et al., 2010). Hence, following plume emplacement segregation of liquids and solids may produce granodiorites and tonalites in upper crustal levels and granulites in the lower crust, which is fairly accounting for the layered structure and composition of the continental crust (Rudnick and Gao, 2003; Taylor and McLennan, 1985). Based on dehydration-melting experiments (on pelite, wacke, tonalite and mafic rocks) it was recently shown, that during sediment subduction/erosion, mafic rocks become eclogite and may sink into the mantle, whereas more silicic rich rocks are transformed into felsic gneisses that are positively to neutrally buoyant and can relaminate the base of the upper crust (Hacker et al., 2011). In addition, recycling of older crustal materials is widely supported by isotope geochemistry (McCulloch and Wasserberg, 1978; Allegre and Ben Othman, 1980).

The possibility that andesite liquids, generated by reaction between slab melts and the mantle wedge (e.g., Kelemen et al., 2003), are fractionated within the continental crust giving rise to silicic batholiths and mafic granulites, cannot be discarded. This hypothesis is compatible with the plume melting model and the melting and melting-reaction experiments of subducted mélanges mentioned above.

4.3. Accretionary wedge, sediment subduction, sediment erosion

Crustal growth at continental margins is either accomplished by arc volcanism or the piling up of accretionary masses of sedimentary deposits and fragments of thicker crustal bodies scraped off the subducting lower plate (von Huene and Scholl, 1991; Le Pichon et al., 1993). The formation of large accretionary prisms is consistent with our experiments of stable and extensional arcs where most incoming sediments are accreted frontally. Enhanced fluid weakening ($\lambda_{fluid} < 0.1$) weakens the sediments accumulated atop the slab within the subduction channel. Hence, sediments do not subduct but decouple from the slab and stack up at the surface forming a growing prism. However crustal material can also bypass the accretionary prism as a result of sediment subduction or can be removed from the upper plate by subduction erosion (von Huene and Scholl, 1991). Sediment subduction occurs in two types of convergent margins: margins where little net accretion takes place (all incoming sediments are subducted) and margins where accretionary prisms form (some incoming sediments are scraped off). Reduced fluid weakening ($\lambda_{fluid} \geq 0.1$) strengthens the sediments atop the slab, which enhances sediment subduction. Von Huene and Scholl (1991) estimated that, where small to medium sized prisms have formed, approximately 20% of the incoming sediment is accreted and a minimum of 80% is subducted. This is in good agreement with our results of compressional arcs, where small to medium sized prisms form. In contrast to sediment subduction, subduction erosion (Scholl, 1987) requires erosion of rocks, which have been part of the upper crust (von Huene and Scholl, 1991). A combination of reduced fluid ($\lambda_{fluid} \geq 0.1$) and enhanced melt weakening ($\lambda_{melt} \leq 0.1$) results in compressional arcs with a weak continental lithosphere. The emplacement of melts within the lower crust enables local extension and facilitates basal erosion,

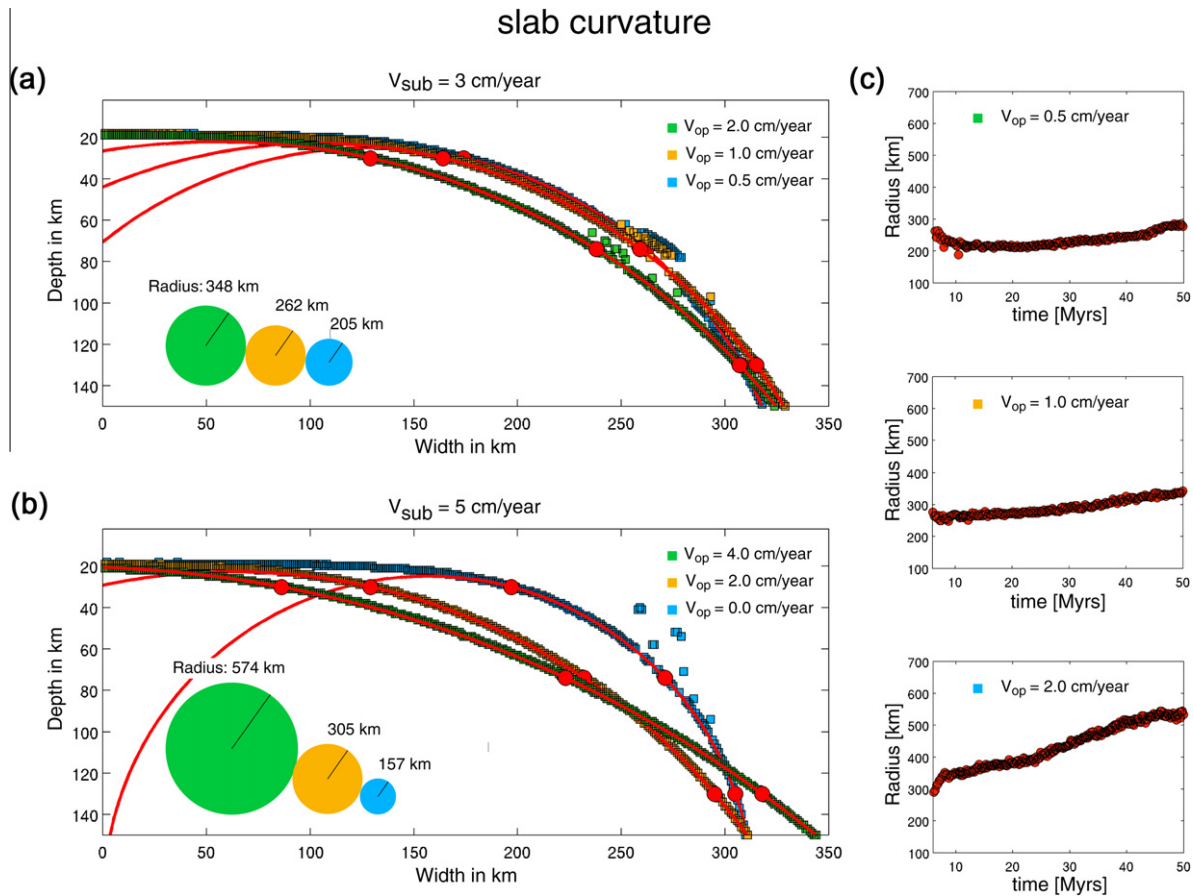


Fig. 13. Radius of the slab curvature after 12 Myrs for (a) slow ($v_{\text{sub}} = 3$ cm/year, Table 2, Nos.: 53, 65, 77) and (b) fast subducting slabs ($v_{\text{sub}} = 5$ cm/year, Table 2, Nos.: 13, 26, 29). The faster the trenchward motion of the upper plate (the higher the convergence rate the bigger the radius of the slab curvature (the shallower the slab dip)). (c) Radius of the slab curvature with time for $v_{\text{sub}} = 3$ cm/year, $v_{\text{op}} = 0.5$ cm/year, $v_{\text{op}} = 1$ cm/year, $v_{\text{op}} = 2$ cm/year (Table 2, Nos.: 13, 26, 29). The radius of the slab curvature increases with time.

whereby the subcrustal underside of the upper crust is removed. The formation of accretionary prisms is thus mainly controlled by weakening effects imposed by fluids and melts. A major assumption in the present study is that weakening takes place in the bulk of the accretionary wedge that is subjected to aqueous fluid percolation. In nature, such fluid flow is likely to be localized (e.g., Moore and Vrolijk, 1992) and our approach, therefore, may not necessarily capture all details of the internal accretion wedge structure. Nevertheless, as demonstrated in a previous study (Gerya and Meilick, 2011) general regimes of accretion wedge dynamics that are characteristic for subduction zones (accretionary versus erosional margins) are reproduced by models with different amounts of fluid-related weakening. Further modifications of accretion wedge dynamics may come from spatial and temporal variations of erosion and sedimentation rates (Simpson, 2010) that are also not accounted for in our study.

4.4. Mode of subduction

Fluids percolating from the subducting slab into the mantle wedge mainly control the coupling of the plates, whereas melts percolating toward the surface weaken the lithosphere above the arc.

Thus two extreme end-members can be defined: (1) extensional arcs with back-arc extension (Fig. 10) and (2) compressional arcs with back-arc compression (Fig. 7), represented by the Mariana and Peruvian-Chilean arcs, respectively. Based on earthquakes studies, Uyeda and Kanamori (1979) argued that there is a

significant difference in the mode of plate motion at interplate boundaries between the two types of trench systems. In the Peruvian and Chilean arcs the plate motion is seismic, in the Mariana it is aseismic. Uyeda and Kanamori (1979) attributed these observations to strong mechanical coupling between the upper and lower plates in the Chilean arc and low or no coupling at the Mariana type boundaries. This difference is manifested in our experiments by tectonic features such as volcanic activity, topography and crustal movement. Compressional arcs are accomplished by flattened, sill-like intrusions in the lower crust, plume development and back-arc compression and trench advance. In contrast, extensional arcs are dominated by decompression melting of dry peridotite, leading to back-arc extension and trench retreat.

4.5. Slab geometry and back-arc stresses

We have shown, that the upper plate motion plays an important role on the slab dip, as well as on the geodynamic setting and the mode of crustal growth. All three major subduction settings (stable arcs, compressional arcs and extensional arcs) are realized for slowly moving upper plates (Fig. 12). If enhanced upper plate velocities are applied ($v_{\text{op}} > 0.5$ cm/year), only stable and compressional arcs are formed, but extensional arcs do not (Fig. 12; Schellart, 2008). The faster the trenchward motion of the upper plate, the shallower the angle of subduction (e.g., van Hunen et al., 2000). Thus extensional arcs do not correlate with shallow dipping slabs. Comparison of different parameters along 159 transects of present day subduction zones (Lallemand and Heuret,

2005) revealed similar observation, which were confirmed by laboratory experiments (Heuret et al., 2007), showing that slab dips correlate with the absolute motion of the overriding plate and back arc stresses. Natural examples of shallow dipping slabs associated with back-arc compression are the Peruvian and Chilean arcs. An example of a steep slab and back arc extension is the Mariana subduction zone.

5. Conclusions

We have investigated numerically geodynamic regimes of crustal growth at active margins. We conclude that:

- Magmatic addition in stable subduction settings is dominated by flattened intrusions in the lower crust and extrusive volcanics at the surface that are derived by partial melting of slab (basalts, gabbro) and mantle components (wet peridotite). Magmatic addition rates are low ($10 \text{ km}^3/\text{km/Myrs}$).
- In compressional arcs magmatic addition is mainly ascribed to partial melting of slab components (basalts, gabbros, sediments) with minor contribution of hydrated mantle. Flattened intrusions are emplaced at lower crustal levels and extrusive volcanics at the surface. In addition, hybrid plumes are formed at asthenospheric depth that transport subducted crustal material (partially molten sediments and basalts) towards the upper crust, which results in moderate magmatic addition rates ($\sim 40\text{--}70 \text{ km}^3/\text{km/Myrs}$).
- Crust formation in an extensional arc setting is associated with decompression melting of dry peridotite, ocean floor development and elevated magmatic addition rates ($>100 \text{ km}^3/\text{km/Myrs}$).

Acknowledgements

The manuscript has been improved by comments from Dave Stegman and an anonymous reviewer.

This work was supported by ETH Research Grants ETH-0807-2, ETH-0807-3, ETH-0609-2, SNF Research Grants 200020-126832, 200020-129487, Crystal2Plate program, SNF ProDoc program 4-D-Adamello and TopoEurope Program.

A.C. acknowledges financial support from Grants CGL2007-63237/BTE and RNM-5378.

References

- Allegre, C.J., Ben Othman, D., 1980. Nd-Sr isotopic relationship in granitoid rocks and continental crust development: a chemical approach to orogenesis. *Nature* 286, 335–341.
- Bigazzi, G., Del, M.A., Maccera, P.G., 1986. A quantitative approach to trace element and Sr isotope evolution in the Adamello Batholith (Northern Italy). *Contributions to Mineralogy and Petrology* 94, 46–53.
- Bittner, D., Schmeling, H., 1995. Numerical modeling of melting processes and induced diapirism in the lower crust. *Geophysical Journal International* 123, 59–70.
- Blundy, J.D., Sparks, R.J.S., 1992. Petrogenesis of mafic inclusions in granitoids of the Adamello Massif, Italy. *Journal of Petrology* 33, 1039–1104.
- Carlson, R.L., Miller, D.J., 2003. Mantle wedge water contents estimated from seismic velocities in partially serpentinized peridotites. *Geophysical Research Letters* 30, 1250.
- Castro, A., Gerya, T.V., García-Casco, A., Fernández, C., Díaz Alvarado, J., Morenó-Ventas, I., Löw, I., 2010. Melting relations of MORB-sediment mélanges in underplated mantle wedge plumes. Implications for the origin of cordilleran-type batholiths. *Journal of Petrology* 51, 1267–1295.
- Castro, A., Gerya, T.V., 2008. Magmatic implications of mantle wedge plumes: experimental study. *Lithos* 103, 138–148.
- Chopra, P.N., Paterson, M.S., 1984. The role of water in the deformation of dunite. *Journal of Geophysical Research* 89, 7861–7876.
- Clauser, C., Huenges, E., 1995. Thermal conductivity of rocks and minerals. In: Ahrens, T.J. (Ed.), *Rock Physics and Phase Relations*. AGU Reference Shelf 3. American Geophysical Union, Washington, DC, pp. 105–126.
- Clemens, J.D., Mawer, C.K., 1992. Granitic magma transport by fracture propagation. *Tectonophysics* 204, 339–360.
- Connolly, J.A.D., 2005. Computation of phase equilibria by linear programming: a tool for geodynamic modeling and its application to subduction zone decarbonation. *Earth and Planetary Science Letters* 236, 524–541.
- Connolly, J.A.D., Podladchikov, Y.Y., 1998. Compaction-driven fluid flow in viscoelastic rock. *Geodinamica Acta* 11, 55–84.
- Daines, M.J., Kohlstedt, D.L., 1994. The transition from porous to channelized flow due to melt/rock reaction during melt migration. *Geophysical Research Letters* 21, 145–148.
- Davies, D., 1983. Mechanics of fold-and-thrust belts and accretionary wedges. *Journal of Geophysical Research* 88, 1153–1172.
- Davis, J.H., 1999. The role of hydraulic fractures in generating intermediate depth earthquakes and subduction zone magmatism. *Nature* 398, 142–145.
- DeCelles, P.G., Ducea, M.N., Kapp, P., Zandt, G., 2009. Cyclicity in Cordilleran orogenic systems. *Nature Geoscience* 2, 251–257.
- Defant, M.J., Drummond, M.S., 1990. Derivation of some modern arc magmas by melting of young subducted lithosphere. *Letters to Nature* 347, 662–665.
- Dimalanta, C., Taira, A., Yumul, G.P., Tokuyama, H., Mochizuki, K., 2002. New rates of western Pacific island arc magmatism from seismic and gravity data. *Earth and Planetary Science Letters* 202, 105–115.
- Drummond, M.S., Defant, M.J., 1990. A model for trondhjemite–tonalite–dacite genesis and crustal growth via slab melting: Archean to modern comparisons. *Journal of Geophysical Research* 95, 21503–21521.
- Elliott, T., Plank, T., Zindler, A., Wjite, W., Bourdon, B., 1997. Element transport from slab to volcanic front at the Mariana arc. *Journal of Geophysical Research* 102, 14991–15019.
- Gerya, T.V., Meilick, F.I., 2011. Geodynamic regimes of subduction under an active margin: effects of rheological weakening by fluids and melts. *Journal of metamorphic Petrology* 29, 7–31.
- Gerya, T.V., Yuen, D.A., 2003. Characteristics-based marker-in-cell method with conservative finite-differences schemes for modeling geological flows with strongly variable transport properties. *Physics of the Earth and Planetary Interiors* 140, 293–318.
- Gerya, T.V., Yuen, D.A., 2007. Robust characteristics method for modelling multiphase visco-elasto-plastic thermo-mechanical problems. *Physics of the Earth and Planetary Interiors* 163, 83–105.
- Gorczyk, W., Willner, A.P., Gerya, T.V., Connolly, J.A.D., Burg, J.-P., 2007. Physical controls of magmatic productivity at Pacific-type convergent margins: numerical modelling. *Physics of the Earth and Planetary Interiors* 163, 209–232.
- Green, T.H., 1980. Island arc and continent-building magmatism – review of petrogenetic models based on experimental petrology and geochemistry. *Tectonophysics* 63, 367–385.
- Hacker, B.R., Kelemen, P.B., Behn, M.D., 2011. Differentiation of the continental crust by remanition. *Earth and Planetary Science Letters* 307, 501–516.
- Hawkesworth, C.J., Turner, S.P., McDermott, F., Peate, D.W., van Calsteren, P., 1997. U–Th isotopes in arc magmas: implications for element transfer from the subducted crust. *Science* 276, 551–555.
- Hawkesworth, C.J., Kemp, A.I.S., 2006. Evolution of the continental crust. *Nature* 443, 811–817.
- Hess, P.C., 1989. *Origin of Igneous Rocks*. Harvard University Press, London, UK.
- Heuret, A., Funiciello, F., Faccenna, C., Lallemand, S., 2007. Plate kinematics, slab shape and back-arc stress: a comparison between laboratory models and current subduction zones. *Earth and Planetary Science Letters* 256, 473–483.
- Hirschmann, M.M., 2000. Mantle solidus: experimental constraints and the effects of peridotite composition. *Geochemistry Geophysics Geosystems* 1. doi:10.1029/2000GC000070.
- Hirth, G., Kohlstedt, D.L., 1996. Water in the oceanic upper mantle: implications for rheology, melt extraction and the evolution of the lithosphere. *Earth and Planetary Science Letters* 144, 93–108.
- Hofmeister, A.M., 1999. Mantle values of thermal conductivity and the geotherm from phonon lifetimes. *Science* 283, 1699–1706.
- Holbrook, W.S., Lizarralde, D., McGeary, S., Bangs, N., Diebold, J., 1999. Structure and composition of the Aleutian island arc and implications for continental crustal growth. *Geology* 27, 31–34.
- Holtzman, B.K., Groebner, N.J., Zimmerman, M.E., Ginsberg, S.B., Kohlstedt, D.L., 2003. Stress-driven melt segregation in partially molten rocks. *Geochemistry Geophysics Geosystems* 4, 8607.
- Holtzman, B.K., Kohlstedt, D.L., 2007. Stress-driven melt segregation and strain partitioning in partially molten rocks: the evolution of melt distribution. *Journal of Petrology* 48, 2379–2406.
- Iwamori, H., 1998. Transportation of H₂O and melting in subduction zones. *Earth and Planetary Science Letters* 160, 65–80.
- Jackson, M.D., Gallagher, K., Petford, N., Cheadle, M.J., 2004. Towards coupled physical and chemical model for tonalite–trondhjemite–granodiorite magma formation. *Lithos* 79, 43–60.
- Johannes, W., 1985. The significance of experimental studies for the formation of migmatites. In: Ashworth, J.R. (Ed.), *Migmatites*. Blackie, Glasgow, UK, pp. 36–85.
- Karato, S.I., Paterson, M.S., FitzGerald, J.D., 1986. Does partial melting reduce the creep strength of the upper mantle? *Nature* 319, 3009–3010.
- Kay, R.W., 1978. Aleutian magnesian andesites: melt from subducted Pacific Ocean crust. *Journal of Volcanology and Geothermal Research* 4, 117–132.
- Kay, R.W., Kay, S.M., 1991. Creation and destruction of the lower continental crust. *Geologische Rundschau* 80, 259–278.
- Kelemen, P.B., Yogodzinski, G.M., Scholl, D.W., 2003. Along-strike variation in lavas of the Aleutian Island arc: implications for the genesis of high Mg# andesite and

- the continental crust. In: Eiler, J.M. (Ed.), *Inside the Subduction Factory*, vol. 138. Geophysical Monograph Ser. American Geophysical Union, Washington, DC, pp. 293–311.
- Kohlstedt, D.L., Zimmerman, M.E., 1996. Rheology of partially molten mantle rocks. *Annual Review of Earth and Planetary Sciences* 24, 41–62.
- Lallemant, S., Heuret, A., 2005. On the relationships between slab dip, back-arc stress, upper plate motion, and crustal nature in subduction zones. *Geochemistry Geophysics Geosystems* 6, Q09006. doi:10.1029/2005GC000917.
- Langmuir, C.H., Klein, E.M., Plank, T., 1992. Petrological systematics of mid-ocean ridge basalts: constraints on melt generation beneath mid-ocean ridges. In: Phipps Morgan, J., Blackman, D.K., Sinton, J.M. (Eds.), *Mantle Flow and Melt generation at Mid Ocean Ridges*, vol. 71. Geophysical Monograph Ser. American Geophysical Union, Washington, DC, pp. 183–280.
- Larter, R.D., Vanneste, L.E., Bruguier, N.J., 2001. Structure, composition and evolution of the South Sandwich island arc: implications for rates of arc magmatic growth and subduction erosion. *EOS Transactions on AGU* 82, F1187.
- Le Pichon, X., Henry, P., Lallemant, S., 1993. Accretion and erosion in subduction zones: the role of fluids. *Annual Review of Earth and Planetary Sciences* 21, 307–331.
- Macera, P., Ferrara, G., Pescia, A., Callegari, E., 1985. A geochemical study on the acid and basic rocks of the Adamello batholith. *Memorie della Società Geologica Italiana* 26, 223–259.
- Mackwell, S.J., Kohlstedt, D.L., Paterson, M.S., 1985. The role of water in the deformation of olivine single crystals. *Journal of Geophysical Research* 90, 319–333.
- Martin, H., Moyen, J.-F., 2003. Secular change in TTG composition: comparison with modern adakites. EGS-AGU-EUG joint meeting, Nice, April, VGP7-1FR20-001.
- Martin, H., Smithies, R.H., Rapp, R., Moyen, J.-F., Champion, D., 2005. An overview of adakite, tonalite-trondhjemite-granodiorite (TTG), and sanukitoid: relationships and some implications for crustal evolution. *Lithos* 79, 1–24.
- McCulloch, M.T., Wasserberg, G.J., 1978. Sm-Nd and Rb-Sr chronology of continental crust formation. *Science* 200, 1003–1011.
- McKenzie, D., 1984. The generation and compaction of partially molten rock. *Journal of Petrology* 25, 713–765.
- McKenzie, D., Bickle, M.J., 1988. The volume and composition of melt generated by extension of the lithosphere. *Journal of Petrology* 29, 625–679.
- Moore, J.C., Vrolijk, P., 1992. Fluids in accretionary prisms. *Reviews of Geophysics* 30, 113–135.
- Moyen, J.-F., 2009. High Sr/Y and La/Yb ratios: the meaning of the “adakitic signature”. *Lithos* 112, 556–574.
- Nikolaeva, K., Gerya, T.V., Connolly, J.A.D., 2008. Numerical Modelling of Crustal Growth in Intraoceanic Volcanic Arcs. *Physics of the Earth and Planetary Interiors* 171, 336–356.
- Pankhurst, R.J., Weaver, S.D., Hereve, F., Larrondo, P., 1999. Mesozoic-Cenozoic evolution of the North Patagonian Batholith in Aysen, southern Chile. *Journal of the Geological Society, London* 156, 673–694.
- Peacock, S.A., 1990. Fluid processes in subduction zones. *Science* 248, 329–337.
- Peacock, S.M., Rushmer, T., Thompson, A.B., 1994. Partial melting of the subducting oceanic crust. *Earth and Planetary Science Letters* 121, 227–244.
- Poli, S., Schmidt, M.W., 2002. Petrology of subducted slabs. *Annual Review of Earth and Planetary Sciences* 30, 207–235.
- Prouteau, G., Scaillet, B., Pichavant, M., Maury, R., 2001. Evidence for mantle metasomatism by hydrous silicic melts derived from subducted oceanic crust. *Nature* 410, 197–200.
- Ranalli, G., 1995. *Rheology of the Earth*. Chapman and Hall, London.
- Reymer, A., Schubert, G., 1984. Phanerozoic addition rates to the continental crust and crustal growth. *Tectonics* 3, 63–77.
- Ringwood, A.E., 1989. Slab-mantle interactions: 3. Petrogenesis of intraplate magmas and structure of the upper mantle. *Chemical Geology* 82, 187–207.
- Rudnick, R.L., 1995. Making continental crust. *Nature* 378, 571–577.
- Rudnick, R.L., Gao, S., 2003. Composition of the continental crust. In: Rudnick, R.L. (Ed.), *The Crust. Treatise on Geochemistry*. Elsevier-Pergamon, Oxford, pp. 1–64.
- Sajona, F.G., Maury, R.C., Bellon, H., Cotten, J., Defant, M.J., Pubellier, M., 1993. Initiation of subduction and the generation of slab melts in western and eastern Mindanao, Philippines. *Geology* 21, 1007–1011.
- Scambelluri, M., Philippot, P., 2001. Deep fluids in subduction zones. *Lithos* 55, 213–227.
- Schellart, W.P., 2008. Overriding plate shortening and extension above subduction zones: a parametric study to explain formation of the Andes Mountains. *Geological Society of America Bulletin* 120, 1441–1454.
- Schmeling, H., Babeyko, A., Enns, A., Faccenna, C., Funicello, F., Gerya, T., Globalek, G., Grigull, S., Kaus, B., Morra, G., van Hunen, 2008. A benchmark comparison of spontaneous subduction models – toward a free surface. *Physics of the Earth and Planetary Interiors* 171, 198–223.
- Schmeling, H., 2006. A model of episodic melt extraction for plumes. *Journal of Geophysical Research* 111. doi:10.1029/2004JB003423.
- Schmeling, H., 2010. Dynamic models of continental rifting with melt generation. *Tectonophysics* 480, 33–47.
- Schmidt, M.W., Poli, S., 1998. Experimentally based water budgets for dehydrating slabs and consequences for arc magma generation. *Earth and Planetary Science Letters* 163, 361–379.
- Scholl, D.W., 1987. Plate tectonics the predictor: the history of wonderments about subduction erosion and sediment subduction – a search for the missing. In: Hilde, T.W.C., Carlson, R.H. (Eds.), *Silver Anniversary Celebration of Plate Tectonics*. Geodynamics Research Institute, Texas A and M Univ, College Station, Texas, pp. 54–56.
- Simpson, G.D.H., 2010. Formation of accretionary prisms influenced by sediment subduction and supplied by sediments from adjacent continents. *Geology* 38, 131–134.
- Sisson, T.W., Bronto, S., 1998. Evidence for pressure-release melting beneath magmatic arcs from basalt at Galunggung, Indonesia. *Letters to Nature* 39, 883–886.
- Sisson, T.W., Layne, G.D., 1993. H₂O in basalt and basaltic andesite glass inclusions from subduction-related volcanoes. *Earth and Planetary Science Letters* 117, 619–635.
- Sizova, E., Gerya, T., Brown, M., Perchuk, L.L., 2010. Subduction styles in the Precambrian: insight from numerical experiments. *Lithos* 116, 209–229.
- Sobolev, A.V., Chaussidon, M., 1996. H₂O concentrations in primary melts from supra-subduction zones and mid-ocean ridges: implications for H₂O storage and recycling in the mantle. *Earth and Planetary Science Letters* 137, 45–55.
- Sobolev, S.V., Babeyko, A.Y., 2005. What drives orogeny in the Andes? *Geology* 33, 617–620.
- Spiegelman, M., Kenyon, P., 1992. The requirements for chemical disequilibrium during magma migration. *Earth and Planetary Science Letters* 109, 611–620.
- Stevenson, D.J., 1989. Spontaneous small-scale melt segregation in partial melts undergoing deformation. *Geophysical Research Letters* 16, 1067–1070.
- Stolper, E., Newman, S., 1994. The role of water in the petrogenesis of Marina trough magmas. *Earth and Planetary Science Letters* 121, 293–325.
- Tatsumi, Y., 1986. Migration of fluid phases and genesis of basalt magmas in subduction zones. *Journal of Geophysical Research* 94, 4697–4707.
- Tatsumi, Y., 2005. The subduction factory: how it operates in the evolving earth. *GSA Today* 15 (7).
- Tatsumi, Y., Eggins, S., 1995. *Subduction Zone Magmatism*. Blackwell, Cambridge.
- Taylor, H.P., 1980. The effects of assimilation of country rocks by magmas on ¹⁸⁰/¹⁶⁰ and ⁸⁷Sr/⁸⁶Sr systematic in igneous rocks. *Earth and Planetary Science Letters* 47, 243–254.
- Taylor, S.R., 1966. The origin and growth of continents. *Tectonophysics* 4, 17–34.
- Taylor, S.R., McLennan, S.M., 1985. *The Continental Crust: Its Composition and Evolution*. Blackwell, Oxford.
- Thompson, A.B., Matile, L., Ulmer, P., 2002. Some thermal constraints on crustal assimilation during fractionation of hydrous, mantle-derived magmas with examples from central Alpine batholiths. *Journal of Petrology* 43, 403–422.
- Tiara, A., Saito, S., Aoike, K., Morita, S., Tokuyama, H., Suyehiro, H., Takahashi, N., Shinohara, M., Kiyokawa, S., Naka, J., Klaus, A., 1998. Nature and growth of the Northern Izu-Bonin (Ogasawara) arc crust and their implications to continental crust formation. *Island Arc* 7, 395–407.
- Turcotte, D.L., Schubert, G., 2002. *Geodynamics*. Cambridge University Press, Cambridge, UK.
- Ulmer, P., Callegari, E., Sonderegger, U., 1985. Genesis of the mafic and ultramafic rocks and their genetical relations to the tonalitic-trondhjemitic granitoids of the southern part of the Adamello batholith (Northern Italy). *Memorie della Società Geologica Italiana* 26, 309–322.
- Uyeda, S., Kanamori, H., 1979. Back-arc opening and the mode of subduction. *Journal of Geophysical Research* 84, 1049–1061.
- Van Hunen, J., van den Berg, A.P., Vlaar, N.J., 2000. A thermomechanical model of horizontal subduction below an overriding plate. *Earth and Planetary Science Letters* 182, 157–169.
- Van Hunen, J., van den Berg, A.P., Vlaar, N.J., 2002. The impact of the South-American plate motion and the Nazca Ridge subduction on the flat subduction below South Peru. *Geophysical Research Letters* 182, 157–169.
- Von Huene, R., Scholl, D.W., 1991. Observations at convergent margins concerning sediment subduction, subduction erosion, and the growth of continental crust. *Review of Geophysics* 29, 279–316.
- Weertman, J., 1971. Theory of water-filled crevasses in glaciers applied to vertical magma transport beneath oceanic ridges. *Journal of Geophysical Research* 76, 1171–1183.
- Wyllie, P.J., 1984. Constraints imposed by experimental petrology on possible and impossible magma sources and products. *Philosophical Transactions of the Royal Society of London A* 310, 439–456.